The Thermodynamics, Kinetics, and Molecular Mechanism of Intramolecular Electron Transfer in Human Ceruloplasmin

Timothy E. Machonkin and Edward I. Solomon*

Contribution from the Department of Chemistry, Stanford University, Stanford, California 94305

Received June 28, 2000. Revised Manuscript Received September 15, 2000

Abstract: Ceruloplasmin is a multicopper oxidase that contains three type 1 Cu sites and a type 2/type 3 trinuclear Cu cluster. All other multicopper oxidases contain only one type 1 Cu and a trinuclear cluster. In oxidized human ceruloplasmin, one type 1 Cu site is reduced and cannot be oxidized, at least in part due at to a high reduction potential, which is not catalytically relevant. Here we have examined the thermodynamics and kinetics of electron transfer among the five redox-active Cu sites to obtain insight into the molecular mechanism of intramolecular electron transfer and the function of the additional, redox-active T1 Cu site. The redox potentials of the Cu sites of human ceruloplasmin were determined by reductive and poised potential titrations. In pH 7.0 phosphate buffer, the potentials of the type 1, type 2, and type 3 Cu sites are 448, 491, and 415 mV, respectively. Cl^- binds to the trinuclear cluster and significantly increases the potentials of the type 2 and type 3 Cu, indicating that Cl^- is a physiologically relevant effector of the redox potentials of the Cu sites. Reductive titrations monitored by EPR indicate that the redox potentials of the two redox-active type 1 Cu sites are the same. Upon reduction and reoxidation with O_2, the trinuclear cluster and 50% of the redox-active type 1 Cu are reoxidized. From EPR, this additional electron is distributed equally between the two redox-active type 1 Cu sites. Rapid freeze−quench EPR demonstrated that the rate of electron transfer between the two T1 Cu sites is $>150\ s^{-1}$, which is faster than the rate of decay of the native intermediate state and indicates that both sites may be catalytically relevant. After reoxidation, the additional electron does not transfer to the trinuclear cluster. Addition of 1−2 equiv of Fe(II) induces ET to the type 2 and T3 Cu sites, indicating that the trinuclear cluster requires at least two electrons to be reduced. Kinetics of reduction of the oxidized enzyme were also studied. Reduction of the type 1 and type 3 Cu sites is fast, while reduction of the type 2 Cu site is slow, indicating that the type 3 Cu pair is reduced by a reduced type 1 Cu and another Fe(II). These results provide new insight into the molecular mechanism of intramolecular electron transfer in ceruloplasmin. Possible electron-transfer pathways among the Cu sites were examined, and the role of two functional type 1 Cu sites is discussed.

Introduction

The multicopper oxidases are an important class of enzymes found in bacteria, fungi, plants, and animals. The best studied members of this class are plant laccase (Lc), fungal Lc, ascorbate oxidase (AO), and mammalian ceruloplasmin (Cp). These enzymes couple the four-electron reduction of O_2 to water with four sequential one-electron oxidations of substrate via a ping-pong mechanism and use three types of Cu sites: type 1 (T1), type 2 (T2), and type 3 (T3).[1] The T1 or blue Cu site is characterized by an intense ligand to metal charge-transfer (LMCT) band at ∼600 nm and narrow parallel hyperfine splitting [$A_{\|} = (43-95) \times 10^{-4}\ cm^{-1}$] in the electron paramagnetic resonance (EPR) spectrum, both of which originate from the highly covalent Cu $d_{x^2-y^2}$ Cys S p_π bond.[2,3] The T1 Cu site in the multicopper oxidases functions in long-range electron transfer (ET), shuttling electrons from substrate to the other Cu sites. The T2 or normal Cu site is characterized by the lack of strong absorption bands and large parallel hyperfine [$A_{\|} = (158-201) \times 10^{-4}\ cm^{-1}$], typical of tetragonal Cu(II). The T3 or coupled binuclear Cu site is characterized by an intense LMCT at ∼330 nm and the lack of an EPR signal due to strong isotropic exchange coupling mediated by a single hydroxide bridge. Together the T2 and T3 Cu sites form a trinuclear Cu cluster that is the site for O_2 reduction.[4−7] Crystal structures now exist for the oxidized[7] and reduced[8] forms of AO, a T2 Cu-depleted form of a fungal Lc,[9] and resting oxidized[10] and metal-,[11] organic substrate-, and N_3^--bound forms[12] of human Cp.

* To whom correspondence should be addressed. Phone or fax: (650) 723-9104. E-mail: edward.solomon@stanford.edu.

(1) Solomon, E. I.; Sundaram, U. M.; Machonkin, T. E. *Chem. Rev.* **1996**, *96*, 2563−2605.

(2) Gewirth, A. A.; Solomon, E. I. *J. Am. Chem. Soc.* **1988**, *110*, 3811−3819.

(3) Solomon, E. I.; Penfield, K. W.; Gewirth, A. A.; Lowery, M. D.; Shadle, S. E.; Guckert, J. A.; LaCroix, L. B. *Inorg. Chim. Acta* **1996**, *243*, 67−78.

(4) Allendorf, M. D.; Spira, D. J.; Solomon, E. I. *Proc. Natl. Acad. Sci. U.S.A.* **1985**, *82*, 3063.

(5) Spira-Solomon, D. J.; Allendorf, M. D.; Solomon, E. I. *J. Am. Chem. Soc.* **1986**, *108*, 5318.

(6) Cole, J. L.; Tan, G. O.; Yang, E. K.; Hodgson, K. O.; Solomon, E. I. *J. Am. Chem. Soc.* **1990**, *112*, 2243−2249.

(7) Messerschmidt, A.; Ladenstein, R.; Huber, R.; Bolognesi, M.; Avigliano, L.; Petruzzelli, R.; Rossi, A.; Finazzi-Agro, A. *J. Mol. Biol.* **1992**, *224*, 179−205.

(8) Messerschmidt, A.; Luecke, H.; Huber, R. *J. Mol. Biol.* **1993**, *230*, 997−1014.

(9) Ducros, V.; Brzozowski, A. M.; Wilson, K. S.; Brown, S. H.; Østergaard, P.; Schneider, P.; Yaver, D. S.; Pedersen, A. H.; Davis, G. J. *Nat. Struct. Biol.* **1998**, *5*, 310−316.

(10) Zaitseva, I.; Zaitsev, V.; Card, G.; Moshov, K.; Bax, B.; Ralph, A.; Lindley, P. *J. Biol. Inorg. Chem.* **1996**, *1*, 15−23.

(11) Lindley, P. F.; Card, G.; Zaitseva, I.; Zaitsev, V.; Reinhammar, B.; Selin-Lindgren, E.; Yoshida, K. *J. Biol. Inorg. Chem.* **1997**, *2*, 454−463.

10.1021/ja002339r CCC: $19.00
Published on Web 12/01/2000

Plant and fungal Lcs contain one of each of the three types of Cu sites; AO is a dimer but otherwise similar. Fungal Lc and AO have a three-domain structure with the T1 Cu site near the surface of domain 3 and coupled via a 13-Å cysteine−histidine ET pathway to trinuclear Cu cluster, which resides at the interface of domains 3 and 1. Cp is unique: it consists of six homologous domains arranged in roughly 3-fold symmetry and contains two additional T1 Cu sites, the roles of which have long been elusive. Like Lc and AO, Cp has a T1 site in the C-terminal domain (domain 6) coupled to the trinuclear cluster via a CysHis pathway ($T1_{CysHis}$).[10] The other two T1 Cu sites are found in domains 4 ($T1_{Remote}$) and 2. The T1 Cu site in domain 2 differs from the others in that it lacks an axial methionine.[13,14] We have recently shown by X-ray absorption spectroscopy, SQUID magnetic susceptibility, and EPR that one of the T1 Cu sites remains permanently reduced (under all currently known conditions), at least in part due to a high reduction potential, and we have assigned it as the T1 Cu site in domain 2 ($T1_{PR}$).[15] Since this site cannot be oxidized, it is not catalytically relevant and is likely a vestige of gene duplication. The other two T1 Cu sites are both redox-active, and both have a divalent metal ion binding (M^{2+}) site adjacent to them and a trivalent metal ion binding site (M^{3+}) located above this and closer to the surface.[11] This implies that both may be involved in the ferroxidase activity of Cp,[16−19] but this has not been proven. For $T1_{Remote}$ to be catalytically relevant, at least two factors must be met: (1) its redox potential must be near that of the other Cu sites, or else it will tend to stay reduced or oxidized during turnover, and (2) the rate of ET in to and out of this site must be reasonably fast. Neither factor is known.

Plant (*Rhus vernicifera*) Lc has been extensively studied, and the key features of its mechanism have been elucidated. Reduction with substoichiometric amounts of reductant yields no new intermediates: the electrons distribute among the Cu sites based upon their relative redox potentials.[20−23] When (and only when[6]) the trinuclear cluster is fully reduced, the enzyme reacts with O_2, yielding a peroxide-level intermediate.[24] Cleavage of the O−O bond then yields the "native intermediate", which lacks a T2 Cu EPR signal but has an unusual high-field EPR signal only seen at <25 K.[25−27] The peroxide intermediate is trapped by substituton of the T1 Cu site with Hg(II) (T1HgLc) but has been shown to be kinetically competent.[28] The decay of the native intermediate to the resting oxidized form and the rate of reduction of the resting oxidized form are too slow to be consistent with steady-state kinetics,[22,23,26,29] while reduction of the native intermediate is much faster,[30] indicating that under turnover the native intermediate is the active oxidized form of plant Lc.[1] This work provides a basis for understanding the mechanism of the other multicopper oxidases.

In Cp, the picture is far less complete and is greatly complicated by the presence of two redox-active T1 Cu sites.[31] The reduction potentials of the two T1 Cu sites[32,33] and the relative redox potentials of the T1 and T3 Cu sites have been reported.[32,34] However, these were often reported under different conditions and are in some cases apparently contradictory. Musci et al. noted that addition of 0.15 M NaCl to human Cp, as isolated by the method of Calabrese and co-workers[35] (which we have shown to contain one additional electron distributed mostly on the T1 and T2 Cu sites[15]), increased the fraction of oxidized T1 Cu and decreased the fraction of oxidized T3 Cu.[36] Reduction of the T1 Cu by Fe(II) is very fast: $>1.2 \times 10^6$ M^{-1} s^{-1}.[37,38] Upon reduction with ascorbate and reoxidation with O_2, all of the T3 Cu reoxidizes within 15 ms.[38] Evidence exists for a native intermediate of Cp, similar to that in Lc.[39,40] The behavior of the T1 coppers upon reoxidation with O_2 is far more complicated and puzzling. Reoxidation of the T1 coppers is sharply biphasic: 55% of the T1 Cu is reoxidizes in 15 ms, but the remaining fraction of T1 Cu does not reoxidize for many hours.[38,41] Addition of Fe(II) enhances the slow phase.[41] From this, it was proposed that two T1 Cu sites had very different properties: both are rapidly reduced with Fe(II), but only one is rapidly reoxidized upon addition of O_2. Reduction of the T1 Cu sites by pulsed radiolytic reduction of the Cys855/Cys881 disulfide bridge followed by subsequent intramolecular ET has been reported.[42] From this it was concluded that there was no intramolecular ET between the T1 Cu sites.

In this study, we have examined the thermodynamics and kinetics of the electron distribution in Cp in a consistent set of physiologically relevant conditions in order to provide a comprehensive picture of the intramolecular ET. We observe the same biphasic kinetics of reoxidation of the T1 coppers, but on the basis of rapid freeze−quench (RFQ) EPR data, we

(12) Zaitsev, V. N.; Zaitseva, I.; Papiz, M.; Lindley, P. F. *J. Biol. Inorg. Chem.* **1999**, *4*, 579−587.
(13) Ortel, T. L.; Takashi, N.; Putnam, F. W. *Proc. Natl. Acad. Sci. U.S.A.* **1984**, *81*, 4761−4765.
(14) Messerschmidt, A.; Huber, R. *Eur. J. Biochem.* **1990**, *187*, 341−352.
(15) Machonkin, T. E.; Zhang, H. H.; Hedman, B.; Hodgson, K. O.; Solomon, E. I. *Biochemistry* **1998**, *37*, 9570−9578.
(16) Lahey, M. E.; Gubler, C. J.; Chase, M. S.; Cartwright, G. E.; Wintrobe, M. M. *Blood* **1952**, *7*, 1053−1074.
(17) Osaki, S.; Johnson, D. A. *J. Biol. Chem.* **1969**, *244*, 5757−5765.
(18) Ragan, H. A.; Nacht, S.; Lee, G. R.; Bishop, C. R.; Cartwright, G. E. *Am. J. Phys.* **1969**, *217*, 1320−1323.
(19) Roeser, H. P.; Lee, G. R.; Cartwright, G. E. *J. Clin. Invest.* **1970**, *49*, 2408−2417.
(20) Reinhammar, B. R. M.; Vänngård, T. I. *Eur. J. Biochem.* **1971**, *18*, 463−468.
(21) Reinhammar, B. R. M. *Biochim. Biophys. Acta* **1972**, *275*, 245−259.
(22) Andréasson, L.-E.; Reinhammar, B. *Biochim. Biophys. Acta* **1976**, *445*, 579−597.
(23) Andréasson, L.-E.; Reinhammar, B. *Biochim. Biophys. Acta* **1979**, *568*, 145−156.
(24) Shin, W.; Sundaram, U. M.; Cole, J. L.; Zhang, H. H.; Hedman, B.; Hodgson, K.; Solomon, E. I. *J. Am. Chem. Soc.* **1996**, *118*, 3202−3215.
(25) Aasa, R.; Brändén, R.; Deinum, J.; Malmström, B. G.; Reinhammar, B.; Vänngård, T. *FEBS Lett.* **1976**, *61*, 115−118.
(26) Andréasson, L.-E.; Bränden, R.; Reinhammar, B. *Biochim. Biophys. Acta* **1976**, *438*, 370−379.
(27) Clark, P. A.; Solomon, E. I. *J. Am. Chem. Soc.* **1992**, *114*, 1108−1110.
(28) Cole, J. L.; Ballou, D. P.; Solomon, E. I. *J. Am. Chem. Soc.* **1991**, *113*, 8544−8546.
(29) Peterson, L. C.; Degn, H. *Biochim. Biophys. Acta* **1978**, *526*, 85−92.
(30) Hansen, F. B.; Koudelka, G. B.; Noble, R. W.; Ettinger, M. J. *Biochemistry* **1984**, *23*, 2057−2064.
(31) Since we have already determined that one of the T1 sites is permanently reduced and not catalytically relevant, from now on we shall only refer to the two redox-active T1 Cu sites.
(32) Deinum, J.; Vänngård, T. *Biochim. Biophys. Acta* **1973**, *310*, 321−330.
(33) Sakurai, T.; Nakahara, A. *Inorg. Chim. Acta* **1986**, *123*, 217−220.
(34) Carrico, R. J.; Malmström, B. G.; Vänngård, T. *Eur. J. Biochem.* **1971**, *20*, 518−524.
(35) Calabrese, L.; Mateescu, M. A.; Carbonaro, M.; Mondovi, B. *Biochem. Int.* **1988**, *16*, 199−208.
(36) Musci, G.; Bonaccorsi di Patti, M. C.; Calabrese, L. *J. Protein Chem.* **1995**, *14*, 611−619.
(37) Osaki, S.; Walaas, O. *J. Biol. Chem.* **1967**, *242*, 2653−2657.
(38) Carrico, R. J.; Malmström, B. G.; Vänngård, T. *Eur. J. Biochem.* **1971**, *22*, 127−133.
(39) Manabe, T.; Manabe, N.; Hiromi, K.; Hatano, H. *FEBS Lett.* **1972**, *23*, 268−270.
(40) Brändén, R.; Deinum, J. *Biochim. Biophys. Acta* **1978**, *524*, 297−304.
(41) de Ley, M.; Osaki, S. *Biochem. J.* **1975**, *151*, 561−566.
(42) Farver, O.; Bendahl, L.; Skov, L. K.; Pecht, I. *J. Biol. Chem.* **1999**, *274*, 26135−26140.

find that *both* T1 Cu sites reoxidize by 50% within 16 ms, implying surprisingly fast intramolecular ET between the two T1 Cu sites. This state does not reequilibrate to the electron distribution determined by reductive titrations. From these results, together with an examination of the rate at which electron distribution is achieved in the reductive titrations, we have formulated a fundamentally new description of the role of the $T1_{Remote}$ Cu site in the mechanism of Cp and of the mechanism of intramolecular ET in the multicopper oxidases in general.

Experimental Section

Water was purified to a resistivity of 15.5−17 MW cm^{-1} with a Barnstead Nanopure deionization system. All other chemicals were reagent grade and used without further purification. Fresh human plasma was obtained from the Stanford Blood Center, and Cp was purified from this by the rapid one-step method[35] modified as previously described.[15] The protein was assayed for purity, protein concentration, and Cu content and was oxidized with H_2O_2 (and the excess H_2O_2 removed) as previously described.[15] All samples of Cp were oxidized with H_2O_2 prior to addition of any other reagents (e.g., NaCl) and were used immediately or kept frozen at −80 °C until use.

Absorption spectra were recorded on a Hewlett-Packard HP8452A diode array UV−visible absorption spectrophotometer in a 1-cm path length cuvette. EPR spectra were obtained with a Bruker ER 220-D-SRC spectrometer. Sample temperatures were maintained at 77 K with a liquid N_2 finger dewar or at ∼8 K with an Air Products Helitran LTR. EPR spectra were spin quantitated with a 1.0 mM aqueous copper standard run in the same tube as the sample where possible.[43] Magnetic circular dichroism (MCD) spectra were obtained in the UV−visible region with a Jasco J-500-C spectropolarimeter operating with an S-20 photomultiplier tube and in the near-IR region with a Jasco J-200-D spectropolarimeter and a liquid nitrogen-cooled InSb detector. The magnetic field was supplied by either an Oxford SM4 or SM4000 7 T superconducting magnetooptical dewar. The MCD sample cells consisted of two quartz disks with a 3-mm rubber spacer, and protein samples for MCD contained ∼60 vol % of glycerol in order to form an optical-quality glass upon freezing. The data were corrected for zero-field baseline effects induced by cracks in the glass by subtracting the corresponding 0-T scan. RFQ EPR samples were made with an Update Instruments System 1000. The samples were frozen in isopentane maintained at a temperature of <−100 °C and then kept in liquid N_2. All other EPR samples were frozen in liquid N_2. Most of the stopped-flow absorption data were obtained with an Applied Photophysics RX2000 with a path length of 1 cm. The tubing system was made anaerobic by washing with a dithionite solution followed by repeated washings with degassed water and/or buffer; O_2 was prevented from leaking in by passage of a stream of N_2 through the system. The temperature was 25 °C. The absorption data were collected on the Hewlett-Packard HP8452A diode array spectrophotometer. The kinetics of reduction of Cp by excess Fe(II) was obtained with an Applied Photophysics SX.18MV stopped-flow UV−visible absorption spectrophotometer with a path length of 1 cm. The system was degassed as described above, with the difference that a N_2-sparged cooling bath was used instead of a stream of N_2. The temperature was either 8 or 25 °C.

Relative reduction potentials of the copper sites were determined by the reductive titration method.[20] A ∼75 μM solution of Cp was degassed by pump-purging at 0 °C under argon and brought into an anaerobic glovebox. A stock solution of reductant, $Fe(NH_4)_2(SO_4)_2 \cdot 6H_2O$, was prepared in the box with water that was previously degassed by multiple freeze−pump−thaw cycles. Both solutions were kept cold until use. A 205-μL aliquot of the protein solution was mixed with an aliquot of reductant solution and transferred to a 1-cm path length anaerobic cuvette with a Teflon stopcock. Absorption spectra were taken at 25 °C over time until the reaction was complete (generally <30 min.). This procedure was then repeated with a fresh 205-μL aliquot of protein and reductant solution for each point in the titration, until all the redox centers were completely reduced. EPR samples were prepared the same way, with the additional step of transferring the cuvette back into the glovebox and then transferring the solution into an EPR tube. Thus, both absorption and EPR data were obtained on the same samples. The samples for RFQ EPR or for examining reduction over time by EPR were handled in a similar manner, only with higher protein concentrations. Absolute reduction potentials of the T1 Cu were obtained by the poised potential method. To a 205-μL sample of degassed ∼50 μM Cp in a 1-cm path length anaerobic cuvette with a Teflon stopcock was added a small quantity of a concentrated stock solution of degassed $K_3[Fe(CN)_6]$ to yield a final concentration of 25 mM. A small quantity of a concentrated stock solution of degassed $K_4[Fe(CN)_6]$ was added, and absorption spectra were taken at 4 °C over time until the reaction was complete (generally >30 min.). Another aliquot of $K_4[Fe(CN)_6]$ was added to the same solution for each point in the titration. The procedure was also done in reverse: first $K_4[Fe(CN)_6]$ was added to a final concentration of 25 mM and $K_3[Fe(CN)_6]$ was titrated in. All sample handling was done in a glovebox. The reductive titration data were fit with macros written with Mathcad (Mathsoft). Kinetics simulations were performed with Ksim.

Calculations of intramolecular ET pathways were performed with the Pathways program based upon the work primarily of Beratan and Onuchic and obtained from Dr. Jefffrey Regan at Cal Tech. In semiclassical Marcus theory, the ET rate constant, k_{ET}, is dependent upon the electronic coupling matrix element, H_{AB}, the driving force, $\Delta G°$, and the reorganization energy.[44] Different models for calculating H_{AB} exist. The isotropic model considers the nature of the intervening medium with a single scalable parameter β and the distance between the sites:[45,46]

$$k_{ET} = 10^{13} \exp(-\beta d) \exp[-(\Delta G° + \lambda)^2/4\lambda kT] \quad (1)$$

The heterogeneous nature of the intervening medium can be explicitly included using the McConnell superexchange model with a tight-binding Hamiltonian.[47] A simple application of this for proteins has been developed by Beratan and Onuchic,[48−56] in which an ET pathway is described as a product of decay factors for the individual covalent bonds, ϵ_C, hydrogen bonds (H-bonds), ϵ_H, and space jumps, ϵ_S, along a given pathway:

$$H_{AB} \propto \prod \epsilon_C \prod \epsilon_H \prod \epsilon_S \quad (2)$$

The coupling decay across one covalent bond, ϵ_C, has been empirically been found to be 0.6. Decay across a space jump is exponential with distance, *R*. Hydrogen bonds are considered equal to covalent bonds; therefore, from heavy atom to heavy atom the coupling decay is ϵ_C^2. Since there are no definitive criteria for deciding what constitutes an H-bond, we have allowed for exponential decay of the ϵ_H term for longer hydrogen bonds. Thus:

(43) Carithers, R. P.; Palmer, G. *J. Biol. Chem.* **1981**, *256*, 7967−7976.

(44) Marcus, R. A.; Sutin, N. *Biochim. Biophys. Acta* **1985**, *811*, 265−322.

(45) Different conventions exist for defining the distance; we have used the convention of Gray and co-workers, in which the distance *d* is the metal-to-metal distance minus 3.0 Å to account for van der Waal's contact (see ref 51).

(46) Gray, H. B.; Winkler, J. R. *Annu. Rev. Biochem.* **1996**, *65*, 537−561.

(47) Newton, M. D. *Chem. Rev.* **1991**, *91*, 767−792.

(48) Beratan, D. N.; Hopfield, J. J. *J. Am. Chem. Soc.* **1984**, *106*, 1584−1594.

(49) Beratan, D. N.; Onuchic, J. N.; Hopfield, J. J. *J. Chem. Phys.* **1987**, *86*, 4488−4498.

(50) Beratan, D. N.; Onuchic, J. N. *Photosynth. Res.* **1989**, *22*, 173−186.

(51) Beratan, D. N.; Onuchic, J. N.; Betts, J. N.; Bowler, B. E.; Gray, H. B. *J. Am. Chem. Soc.* **1990**, *112*, 7915−7921.

(52) Onuchic, J. N.; Beratan, D. N. *J. Chem. Phys.* **1990**, *92*, 722−733.

(53) Beratan, D. N.; Betts, J. N.; Onuchic, J. N. *Science* **1991**, *252*, 1285−1288.

(54) Beratan, D. N.; Betts, J. N.; Onuchic, J. N. *J. Phys. Chem.* **1992**, *96*, 2852−2855.

(55) Betts, J. N.; Beratan, D. N.; Onuchic, J. N. *J. Am. Chem. Soc.* **1992**, *114*, 4043−4046.

(56) Regan, J. J.; Onuchic, J. N. *Adv. Chem. Phys.* **1999**, *107*, 497−553.

$$\epsilon_C = 0.6 \quad (3)$$

$$\epsilon_S = \epsilon_C \exp[-1.7(R - 1.4)] \quad (4)$$

$$\epsilon_H = \epsilon_C, \quad R = 2.1 \text{ Å}$$

$$\epsilon_H = \epsilon_C \exp[-1.7(R - 2.8)], \quad R > 2.1 \text{ Å} \quad (5)$$

In eq 5, R is the H-atom to H-bond accepting heavy atom distance. The Pathways program implements the above model for a protein structure coordinate file and determines the most favorable ET pathways. The crystal structure of human Cp was obtained from the Protein Data Bank (1KCW), and protons were added with Insight II. The coupling of the metal d-orbitals in to and out of the pathway was set equal to 1. We will consider the effect of differences in metal−ligand bonding (i.e., anisotropic covalency) in electron-transfer rates in the Discussion.

Results and Analysis

Thermodynamics of Intramolecular Electron Transfer. 1. Reductive Titrations in pH 7.0 Phosphate Buffer. The equilibrium distribution of electrons in partially reduced human Cp was determined by reductive titrations[32,34] under the following conditions: pH 7.0 in either phosphate or MOPS buffer, without and with Cl^-. Fe(II) was chosen as the reductant. At pH 7.0, Cp reacts extremely slowly with other reductants such as ascorbate, which would introduce artifacts due to the limited stability of Cp. Since Cp binds divalent metal ions,[11,37,57−59] the potential of Fe in the system is that of Fe bound to the protein and is therefore not known. However, upon addition of >5.0 equiv of Fe(II), we observed no further spectroscopic changes, indicating that reduction of the Cu sites by Fe(II) is stoichiometric; i.e., the reduction potential of Fe(III) is much lower than that of the Cu sites. Also note that although one might expect the Fe(III) thus generated to precipitate, this does not occur, likely due to the low concentrations involved and to the ability of Cp to bind metal ions.[11] The production of Fe(III) generated a new LMCT band at ∼310 nm, a $g_{eff} = 4.3$ signal in the EPR spectrum, and a new EPR feature at ∼3500 G. Since this is the only feature seen in the 2500−3700-G range in samples to which stoichiometric or excess Fe(II) is added, it could easily be subtracted from samples with < 5.0 equiv of Fe(II).

Figure 1A shows the number of oxidized T1, T2, and T3 coppers present in Cp upon addition of 0−5.3 equiv of Fe(II) in pH 7.0 phosphate buffer. The results obtained by absorption spectroscopy are shown by the solid symbols. The total number of oxidized T1 coppers was quantitated from the intensity of the 610-nm band. The Fe(III) LMCT band that grows in at ∼310 nm obscures the 330-nm band of the T3 Cu pair. However, it is negligible at 360 nm, where the T3 Cu band is still sufficiently intense, so this was used to quantitate the amount of oxidized T3 Cu. The amount of oxidized T2 Cu was calculated based upon the difference between the amount of Fe(II) added and the amount of T1 and T3 Cu reduced. Upon addition of 3 equiv of Fe(II), all of the T2 Cu is reduced, most of the T1 Cu is reduced, and nearly all of the T3 Cu is oxidized. This indicates that, in these conditions, the T3 Cu pair has the lowest potential and the potential of the T1 Cu is significantly higher.

Figure 2A shows the EPR spectra of human Cp upon addition of 0−5.3 equiv of Fe(II). The high-field feature due to Fe(III) has been subtracted. The three EPR-active Cu sites are clearly distinguishable: the T2 Cu has an $m_s = -3/2$ hyperfine peak at 2755 G and an off-axis turning point at ∼3405 G, and the two T1 Cu sites have $m_s = -3/2$ hyperfine peaks at 2918 and 2954 G, here called T1A and T1B, respectively. The intensity of these features can be used to determine the fraction of each Cu site that is oxidized. The number of the non-EPR-active oxidized T3 Cu can be determined by difference. These results are shown in Figure 1A as the open symbols. These data indicate that the intensity of the T2 Cu determined by EPR does not mirror that determined by absorption data. We ascribe this to a freezing effect: since the T2 and T3 Cu are in close proximity, small structural changes induced upon freezing would have the greatest effect upon the relative redox potentials of these Cu sites. Examination of the EPR spectra yields several important results: (1) no new EPR signals are observed, (2) the intensities of the T1 Cu EPR features do follow the room-temperature absorption data, and most importantly, (3) both of the T1 Cu features diminish to the *same extent* upon addition of reductant. This indicates that, under these conditions, both T1 Cu sites have the same or very similar reduction potentials.

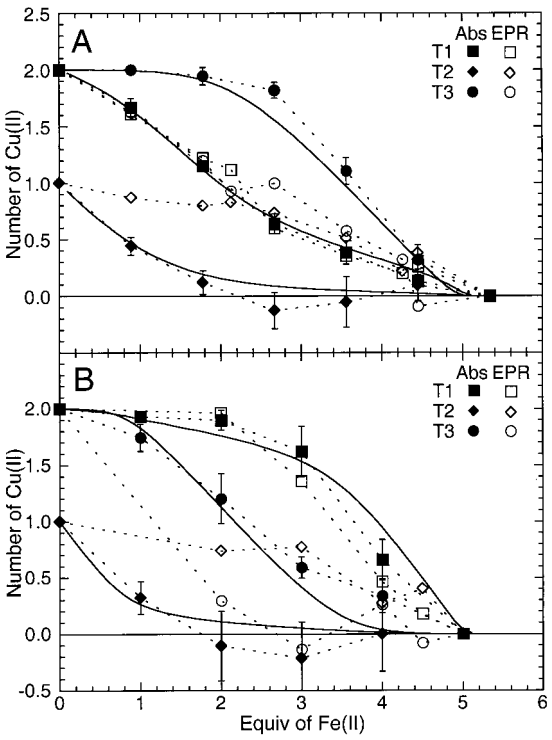

Figure 1. Anaerobic reductive titrations of oxidized human Cp with Fe(II) monitored by absorption and EPR. Conditions: (A) pH 7.0 phosphate buffer; (B) pH 7.0 phosphate buffer plus 0.15 M NaCl. Number of oxidized coppers determined by absorption: (■) T1 Cu, (◆) T2 Cu, and (●) T3 Cu. Number of oxidized coppers determined by EPR: (□) T1 Cu, (◇) T2 Cu, and (○) T3 Cu. Solid lines are the fits to the absorption data calculated from a set of coupled Nernst equations incorporating the differences in the redox potentials among the Cu sites.

The above provides relative potentials for the Cu sites; to obtain actual values of $E°$, the reduction potential of the T1 Cu was determined by the poised potential method. The results at pH 7.0 in phosphate buffer are shown in Figure 3 as solid symbols. The experiment was performed both by starting with 23.2 mM $K_3[Fe(CN)_6]$ and titrating in $K_4[Fe(CN)_6]$ and starting with 23.2 mM $K_4[Fe(CN)_6]$ and titrating in $K_3[Fe(CN)_6]$. From a linear least-squares fit to the data, a reduction potential of 448 ± 10 mV was determined. No evidence of sigmoidal behavior was observed. Therefore, under these conditions, both

(57) Osaki, S. *J. Biol. Chem.* **1966**, *241*, 5053−5059.
(58) Huber, C. T.; Frieden, E. *J. Biol. Chem.* **1970**, *245*, 3973−3978.
(59) McKee, D. J.; Frieden, E. *Biochemistry* **1971**, *10*, 3880−3883.

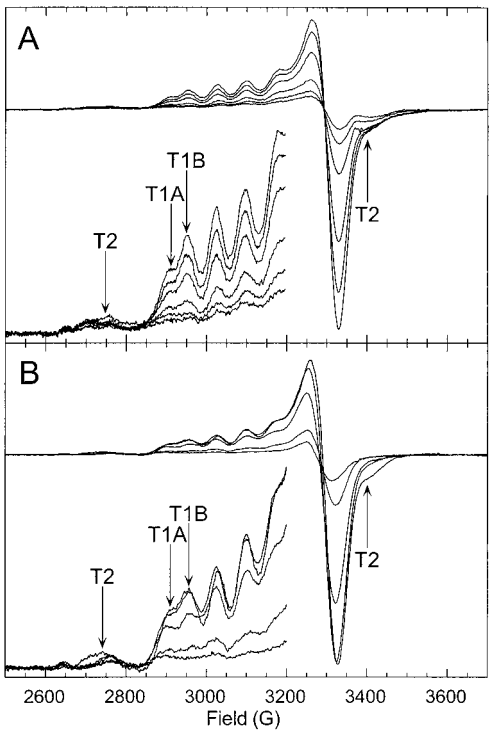

Figure 2. (A) EPR spectra of human Cp in pH 7.0 phosphate buffer with 0, 0.9, 1.8, 2.7, 3.6, 4.5, and 5.3 equiv of Fe(II); microwave frequency, 9.482 GHz. (B) EPR spectra of human Cp in pH 7.0 phosphate buffer plus 0.15 M NaCl with 0, 2.0, 3.0, 4.0, and 4.5 equiv of Fe(II); microwave frequency, 9.478 GHz. Other conditions: temperature, 77 K; microwave power, 20 mW; modulation amplitude, 16 G; modulation frequency, 100 kHz; time constant, 0.5 s.

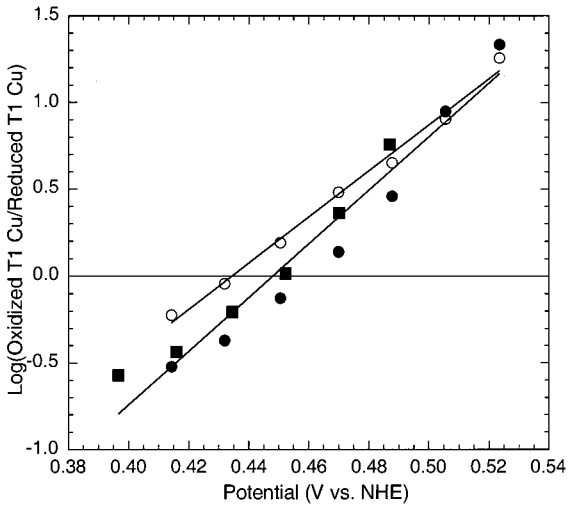

Figure 3. Poised potential titration of human Cp at 4 °C. Conditions are as follows: (●) pH 7.0 phosphate buffer, starting with 23.2 mM $K_3[Fe(CN)_6]$ and titrating in $K_4[Fe(CN)_6]$, (■) pH 7.0 phosphate buffer, starting with 23.2 mM $K_4[Fe(CN)_6]$ and titrating in $K_3[Fe(CN)_6]$, and (○) pH 7.0 phosphate buffer with 0.15 M NaCl, starting with 23.2 mM $K_3[Fe(CN)_6]$ and titrating in $K_4[Fe(CN)_6]$.

T1 Cu sites have a potential of ∼448 mV. This is in agreement with the results from the EPR reductive titration, although the quality of the poised potential data is insufficient to rule out a small difference in T1 Cu potentials.

2. Reductive Titrations in pH 7.0 Phosphate Buffer With Cl^-. The same set of experiments was performed with human Cp in pH 7.0 phosphate buffer with 0.15 M NaCl. Note that the normal range of Cl^- concentration in plasma is 0.101−0.111 M.[60] The numbers of oxidized T1, T2, and T3 coppers upon addition of 0−5.0 equiv of Fe(II) as determined by absorption spectroscopy are shown as the solid symbols in Figure 1B. Upon addition of 3 equiv of Fe(II), all of the T2 Cu and most of the T3 Cu is reduced, while nearly all of the T1 Cu is oxidized. This shows that a physiologically relevant concentration of Cl^- dramatically alters the relative reduction potentials of the Cu sites: now, the T1 coppers have the lowest potential and the potential of the T3 Cu is significantly higher. Thus, addition of Cl^- causes the electron distribution in partially reduced Cp to shift from mostly reduced T1 Cu to mostly reduced T2/T3 Cu.

The EPR spectra of Cp in pH 7.0 phosphate buffer with 0.15 M NaCl upon addition of 0−5.0 equiv of Fe(II) are shown in Figure 2B. These data show that the amount of oxidized T1 Cu in the EPR spectra tracks with the amount observed by absorption (Figure 1B, open symbols) and that both T1 Cu features diminish by the same amount (Figure 2B). Thus, in the presence and absence of Cl^-, both T1 Cu sites have the same or very similar redox potentials. However, the EPR spectra of partially reduced Cp in the presence of Cl^- show marked differences in the T2 Cu signal: the off-axis turning point at ∼3405 G is largely gone, and the $m_s = -3/2$ hyperfine line has become narrower and shifted upfield by ∼20 G (Figure 2B). This is similar to what was observed in the EPR spectrum of as-isolated (i.e., partially reduced) Cp in the presence of Cl^- reported by Musci et al. and interpreted as a half-met T3 Cu.[36] Since the EPR parameters of this signal now differ from that of the oxidized enzyme, the same features cannot be used to quantitate the amount of oxidized T2 Cu. Instead, the amount was determined by double integration and subtraction of the amount of oxidized T1 Cu. The amount of oxidized T3 Cu was determined as described above. These results are shown in Figure 1B as the open symbols. Again, there is a discrepancy between the amount of oxidized T3 Cu as determined by absorption and EPR. We find no basis for assigning the new paramagnetic Cu signal seen in partially reduced Cp in the presence of Cl^- as half-met T3. The intensity of this feature tracks the disappearance of the typical T2 Cu signal (vide infra) and the reduction of the EPR-nondetectable T3 Cu. Furthermore, the discrepancy in the amount of oxidized T2 and T3 Cu between room-temperature absorption and low-temperature EPR was also observed in the absence of Cl^- where no new EPR signal appeared. The new EPR signal is therefore best ascribed to an alteration of the T2 Cu that occurs upon reduction of the adjacent T3 Cu pair.

The reduction potential of the T1 Cu in pH 7.0 phosphate buffer with 0.15 M NaCl was determined by the poised potential method (Figure 3, open symbols). A linear least-squares fit to the data yields a potential of 434 ± 10 mV. As in the absence of Cl^-, no sigmoidal behavior was observed, and both T1 Cu sites appear to have the same potential, consistent with the EPR data. Therefore, addition of Cl^- induces a slight decrease in the redox potential of both T1 Cu sites.

3. Spectroscopic Evidence of Cl^- Binding. Since the addition of Cl^- affects the relative potentials of the T1 and T3 Cu sites in Cp, changes in the spectroscopic features of the Cu sites upon addition of Cl^- to the oxidized enzyme were also examined. No differences were observed in the absorption spectrum (data not shown). Figure 4A shows the EPR spectra of oxidized Cp with and without Cl^-. These spectra clearly show that addition of Cl^- induces an upfield shift to both the $m_s = -3/2$ hyperfine line (Figure 4A) and the off-axis turning point

(60) Tilton, R. C.; Balows, A.; Hohnadel, D. C.; Reiss, R. F. *Clinical Laboratory Medicine*; Mosby: St. Louis, MO, 1992.

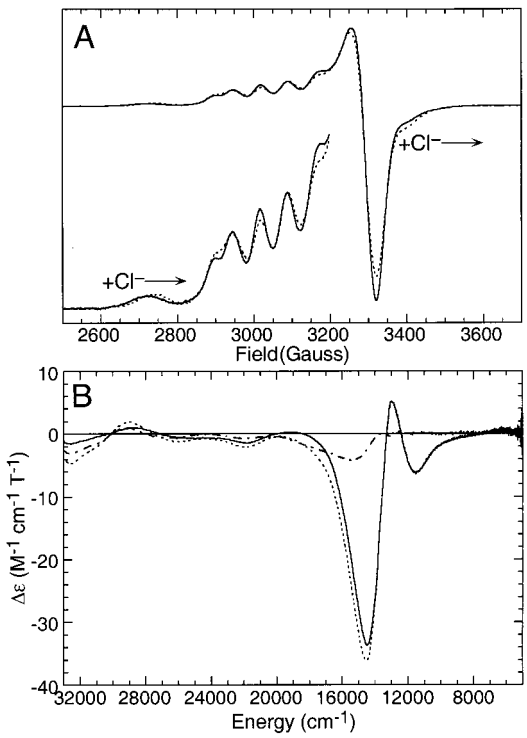

Figure 4. (A) EPR spectra of human Cp in pH 7.0 phosphate buffer without (—) and with (- - -) 0.15 M NaCl. Conditions: microwave frequency, 9.482 GHz; temperature, 77 K; microwave power, 20 mW; modulation amplitude, 16 G; modulation frequency, 100 kHz; time constant, 0.5 s. (B) MCD spectra of human Cp in pH 7.0 phosphate buffer without (—) and with (- - -) 0.15 M NaCl and the difference spectrum of with Cl^- minus without (—•—). Conditions: temperature, 5.0 K; field, 7.0 T.

of the T2 Cu site of ~20 G. Note that the changes to the T2 Cu EPR signal upon reduction of the T3 Cu in the presence of Cl^- are distinct from the change in the oxidized enzyme. Figure 4B shows the MCD spectra of oxidized Cp with and without Cl^- as well as the difference spectrum. Significant changes are clearly evident in the ligand field (LF) region below 20 000 cm^{-1}. Since the T2 Cu MCD features are much weaker than and largely overlap with the T1 LF transitions, it is difficult to ascribe these changes to a single Cu site.

Since, upon addition of Cl^-, the largest effect on the redox potentials is seen for the T3 Cu and the largest spectroscopic changes to both the fully oxidized and partially reduced enzymes are observed for the T2 Cu, it appears that Cl^- directly interacts with the trinuclear cluster, binding to the T2 Cu and possibly bridging the T2 and T3 in the oxidized state. Note that Musci et al. reported an apparent K_d of ~4 mM.[36] Cl^- is expected it to preferentially bind to and stabilize Cu(I) relative to Cu(II), which would explain the increased potential of the T3 Cu pair. Also, the greater binding affinity of Cl^- to the reduced T3 Cu pair would be consistent with the additional changes in the T2 Cu EPR features upon reduction of the T3 Cu.

4. Reductive Titrations in pH 7.0 MOPS Buffer with and without Cl^-. The choice of buffer has been reported to affect the reduction behavior of Cp;[34] therefore, we examined the relative redox potentials of the Cu sites in pH 7.0 MOPS buffer. In MOPS, the Fe(III) band obscures the 330-nm band of the T3 Cu pair. Therefore, to quantitate the number of oxidized T3 coppers, either the deviations from linearity in the increase in the 330-nm band were monitored or, after reduction, the sample was exposed to air. Since the T3 band returns upon reoxidation, the change at 330 nm upon reoxidation measures the fraction

Scheme 1

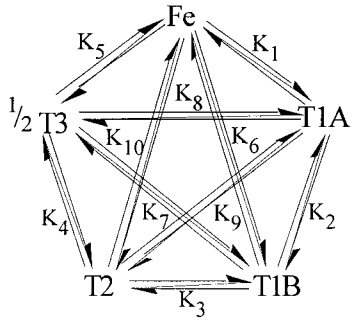

of T3 Cu that was reduced. Both methods gave similar results, but neither was entirely reliable due to the intensity of the Fe(III) band and protein instability. These data, without and with 0.15 M Cl^-, are shown in Figure S1 of the Supporting Information. In the absence of Cl^-, the relative redox potentials of the T1 and T3 Cu sites are intermediate between those in phosphate buffer (T3 Cu lowest) and phosphate plus Cl^- (T1 Cu lowest). In the MOPS with Cl^-, the shape of the titration curve for the T1 Cu closely mirrors that obtained in phosphate plus Cl^-. This demonstrates that Cl^- has the dominant effect on the relative potentials, shifting them to the same values irrespective of buffer.

5. Analysis of the Redox Potential Data. The curves obtained from the reductive titrations were fit to a series of coupled Nernst equations to determine the difference in redox potentials among the Cu sites. This, together with the T1 Cu potentials obtained from the poised potential experiments, were used to determine absolute redox potentials for each of the Cu sites (although note that the reductive titration and poised potential data were obtained at different temperatures, which may have an effect). It was assumed that there is no cooperativity, i.e., that the potential of one Cu site is not affected by the redox state of the others. The assumption that the Cu sites do not interact is almost assuredly an oversimplification (note, for example, the shift in the fraction of oxidized T2 and T3 Cu determined by room-temperature absorption and low-temperature EPR); however, inclusion of even one such interaction potential yields a greatly underdetermined problem. The room-temperature absorption titrations are adequately fit without cooperativity, so it is not such a defining feature that it is required to fit the data. Also, each Cu site is assumed to be in equilibrium with all of the other Cu sites. This issue will be reexamined in the subsequent sections. Given these assumptions, the four Cu sites, T1A, T1B, T2, and T3 (a two-electron acceptor) and the Fe(II/III) couple are related by 10 equilibrium constants, only 4 of which are needed to define the system.

These four equilibria, together with mass balance, yield five equations with five unknowns that can readily be solved with Mathcad. The potentials of both T1 Cu sites in phosphate buffer (which are the same from the EPR reductive titrations) are 448 mV versus NHE based upon the poised potential experiment. From the fits to the reductive titration by absorption (Figure 1A, solid lines), the potential of the T3 Cu site is 33 mV lower than the T1 Cu, yielding a value of 415 mV, and the T2 Cu is 43 mV higher, yielding a value of 491 mV. The shape of the reductive titration T1 Cu curve cannot be adequately fit if the difference in potential between the two T1 Cu sites is more than 22 mV. In phosphate buffer plus Cl^-, the potential of the two T1 Cu sites (which are, again, the same from the EPR reductive titrations) is 434 mV versus NHE based upon the poised potential experiment. The fits to the reductive titration by absorption (Figure 1B, solid lines) yield a potential of the

Table 1. Reduction Potentials of the Cu Sites of Human Cp in Phosphate Buffer and in Phosphate Buffer Plus Cl^-

Cu site	$E°$ in phosphate buffer (mV vs NHE)	$E°$ in phosphate buffer plus Cl^- (mV vs NHE)
T1A	448	434
T1B	448	434
T2	491	539
T3	415	482

T3 Cu site 48 mV above the T1 Cu (482 mV) and a potential of the T2 Cu 105 mV above the T1 Cu (482 mV). Since, in phosphate buffer plus Cl^-, the T1 Cu sites have the lowest potential, the simulation is not very sensitive to differences between the two T1 Cu site potentials. In both sets of conditions, the data were best fit with the T3 Cu acting as a two-electron acceptor. Also, since the potential of the T2 Cu differs the most from that of the others, the simulations are also not very sensitive to changes in this value. These results are summarized in Table 1.

The present study successfully combines reductive titration and poised potential results to obtain the first quantitative determination of the redox potentials of all the Cu sites in Cp under a consistent set of conditions (Table 1). This includes an estimate of the T2 redox potential; the only other reported is for plant Lc.[20,21] Most importantly, our EPR data conclusively show that the two T1 Cu sites have the same redox potential, a result further supported by our other data. This generates a dramatically different picture of the thermodynamics of intramolecular ET in Cp than was previously supposed[32,41] and satisfies one condition for both T1 Cu sites to be relevant in the catalytic cycle. The data in phosphate buffer without Cl^- yield the somewhat surprising result that in partially reduced Cp the T2 Cu is largely reduced and the T3 Cu entirely oxidized. Given that the function of the T1 Cu is to transfer electrons from substrate to the trinuclear cluster, this means the ET from the T1 to the T3 Cu will be slightly energetically unfavorable. This is the opposite of what was seen in plant Lc.[20,21] Addition of Cl^- shifts the trinuclear Cu cluster to higher potential, resulting in T1 to T3 ET that is energetically favorable. Therefore, we conclude that Cl^- is an important physiologically relevant effector of the redox potentials in human Cp.

Kinetics of Intramolecular Electron Transfer. 1. Kinetics of ET upon Reoxidation With O_2. The kinetics of intramolecular ET after reoxidation of reduced human Cp with O_2 were examined in order to determine the possible role of the $T1_{Remote}$ Cu site. Since the reduced enzyme contains five reduced redox-active coppers and reduction of O_2 is a four-electron process, upon reoxidation the enzyme will still contain one extra electron, the distribution of which among the Cu sites can then be monitored by absorption and EPR. As reported previously,[38,41] ~50% of the 610-nm band and all of the 330 nm returned very quickly (<0.1 s); subsequently, the 610-nm band increased gradually over the next several hours. The absorption spectra of resting oxidized and fully reduced Cp, as well as Cp several minutes after reoxidation with O_2 (volume-normalized) are shown in Figure S2A. This demonstrates that, upon reaction with O_2, the T3 Cu pair and ~50% of the T1 Cu are reoxidized.

EPR spectra were obtained on samples of Cp in phosphate buffer frozen >30 s after reaction with O_2-saturated buffer. Representative data are shown in Figure 5A, along with a spectrum of the resting oxidized form (volume-normalized). This spectrum shows that all of the T2 Cu (seen clearly from the $m_s = -3/2$ hyperfine peak at 2755 G and the off-axis turning point at ~3405 G) has reoxidized and the EPR parameters of this site have not changed. Also, the double-integrated intensity is

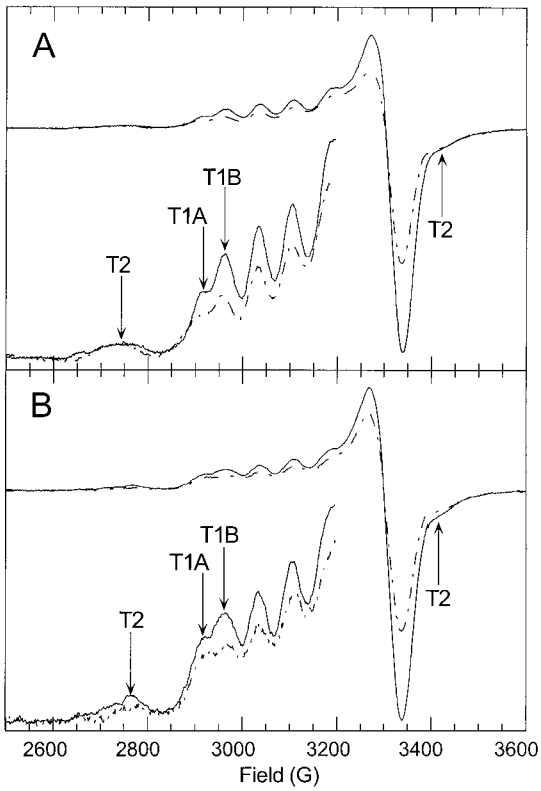

Figure 5. (A) EPR spectra of human Cp in pH 7.0 phosphate buffer in the resting oxidized (—) and reoxidized with O_2 (—·—) states; microwave frequency, 9.505 GHz. (B) EPR spectra of human Cp in pH 7.0 phosphate buffer with 0.15 M NaCl in the resting oxidized (—) and reoxidized with O_2 (—·—) states; microwave frequency, 9.507 GHz. Other EPR conditions: temperature, 77 K; microwave power, 20 mW; modulation amplitude, 16 G; modulation frequency, 100 kHz; time constant, 0.5 s.

~$^2/_3$ that of the resting oxidized form, indicating that ~50% of the T1 Cu has reoxidized, consistent with the absorption data. The EPR spectrum in Figure 5A reveals a crucial new result: the $m_s = -3/2$ hyperfine lines of *both* T1 Cu sites are present in approximately *equal* amounts. This indicates that, at relatively long times (>30 s), both T1 Cu sites have reoxidized by ~50%. Presumably, this arises from O_2 completely reoxidizing one T1 Cu site ($T1_{CysHis}$) followed by ET from the other T1 Cu site ($T1_{Remote}$). Since the T1 Cu sites have the same redox potential, the system equilibrates (in the absence of any ET to the trinuclear cluster, vide infra) to yield 50% of the molecules with $T1_{CysHis}$ reduced and 50% with $T1_{Remote}$ reduced. This is a very different picture of the reoxidation behavior of the Cu sites in Cp than was earlier presumed based solely on stopped-flow absorption[41] or pulsed radiolysis absorption data.[42]

The rate of this intramolecular ET was then studied by RFQ EPR. Representative RFQ EPR spectra of Cp reoxidized with O_2 in phosphate buffer at room temperature are shown in Figure 6. The EPR spectrum at 77 K, 20 mW of microwave power, of the sample frozen 20 ms after mixing with O_2-saturated buffer shows the complete absence of the T2 Cu signal and the presence of both T1 Cu $m_s = -3/2$ hyperfine lines in approximately equal proportion (Figure 6A). The EPR spectrum at ~8 K, 100 mW of microwave power, of this sample is dominated by an intense, broad, negative signal at ~3550 G (Figure 6C). This signal is very similar to the native intermediate signal seen in Lc, which from MCD spectroscopy has been assigned as an oxidized trinuclear cluster with an additional O_2-derived bridging ligand between the T2 and T3 Cu sites yielding

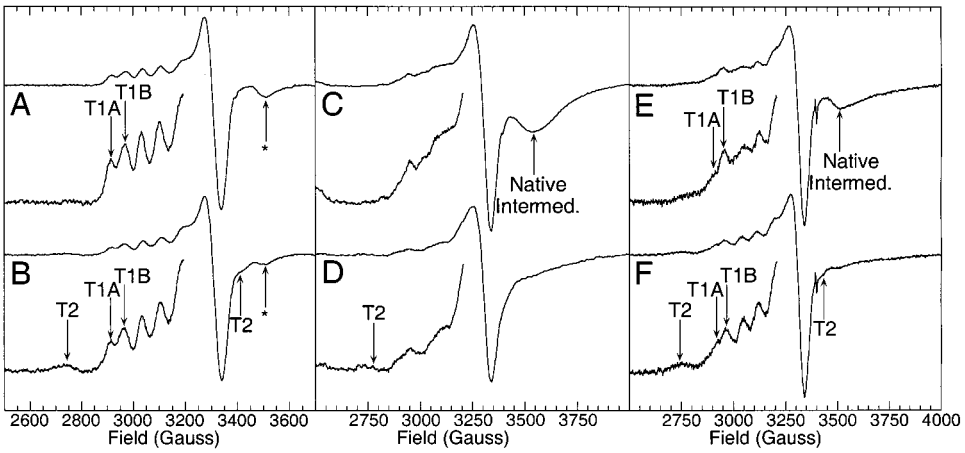

Figure 6. RFQ EPR spectra of human Cp in pH 7.0 phosphate buffer upon reoxidation with O_2. (A) Frozen 20 ms after reoxidation, spectrum taken at 77 K, 20 mW of microwave power (* denotes Fe(III) signal). (B) Frozen 1.0 s after reoxidation, spectrum taken at 77 K, 20 mW of microwave power (* denotes Fe(III) signal). (C) Frozen 20 ms after reoxidation, spectrum taken at ~8 K, 100 mW of microwave power. (D) Frozen 1.0 ms after reoxidation, spectrum taken at ~8 K, 100 mW of microwave power. (E) Frozen 20 ms after reoxidation, spectrum taken at ~8 K, 10 μW of microwave power. (F) Frozen 1.0 s after reoxidation, spectrum taken at ~8 K, 10 μW of microwave power. Other EPR conditions for spectra A and B: microwave frequency, 9.515 GHz; modulation amplitude, 16 G; modulation frequency, 100 kHz; time constant, 0.5 s. Other EPR conditions for spectra C−F: microwave frequency, 9.517 GHz; modulation amplitude, 16 G; modulation frequency, 100 kHz; time constant, 0.5 s.

a $S = {}^1/_2$ ground state delocalized over all three coppers.[27] We therefore assign it as the native intermediate of Cp. The EPR spectrum at ~8 K, 10 μW of microwave power, of the 20-ms sample shows that the T1 Cu features are more prominent at low microwave power due to the slower relaxation rate of the T1 Cu versus the native intermediate signal (Figure 6E). RFQ EPR data were also obtained on samples prepared at ~0 °C frozen 16 ms after mixing with O_2-saturated buffer and prepared at room temperature frozen 60 ms after mixing. These spectra were essentially identical to those shown in Figure 6A, C, and E (data not shown). Thus, at very fast times (16−60 ms), the trinuclear cluster has completely reoxidized, yielding the same native intermediate signal observed in plant Lc. Furthermore, these data demonstrate that, at 16 ms, the extra electron has already equilibrated between the two T1 Cu sites. Assuming that this event is purely $T1_{Remote}$ Cu to $T1_{CysHis}$ Cu ET (i.e., initial reaction with O_2 to generate the native intermediate and reoxidized $T1_{CysHis}$ Cu is extremely rapid and there is no direct $T1_{Remote}$ to trinuclear ET), and assuming that the reaction is at least 90% complete at 16 ms, this puts a lower limit on the rate of this intramolecular ET of 150 s^{-1}.

The EPR spectrum at 77 K, 20 mW of microwave power, of the sample frozen 1.0 s after mixing with O_2-saturated buffer shows that the T2 Cu signal has reappeared and that both T1 Cu $m_s = -{}^3/_2$ hyperfine lines are still present in approximately equal proportion (Figure 6B), in agreement with the results obtained on samples frozen after >30 s (Figure 5A). The EPR spectrum at ~8 K, 100 mW of microwave power, of this sample is dominated by the T2 Cu signal (Figure 6D), as seen in the resting oxidized form of Cp (data not shown). In the EPR spectrum at ~8 K, 10 μW of microwave power (Figure 6F), the T1 Cu features are again more prominent than at high microwave power due to their slower relaxation rate. Given that the native intermediate is still present at 60 ms but essentially gone by 1.0 s, the $t_{1/2}$ for decay of the native intermediate of Cp is in the 200−500-ms range. The fact that the extra reducing equivalent has already equilibrated between the two T1 Cu sites (i.e., in 50% of the molecules, the $T1_{Remote}$ Cu site is oxidized) before the native intermediate has decayed is important, since in plant Lc the native intermediate is believed to be the active oxidized form of the enzyme under turnover. Thus, the $T1_{Remote}$ Cu site satisfies a second condition for catalytic relevance: ET in to and out of this site is fast.

The effect of Cl^- on the reoxidation behavior was also determined. The results were essentially the same: by absorption spectroscopy, ~50% of the 610-nm band and all of the 330 nm returned very quickly (<0.1 s), and the 610-nm band increased only very slowly thereafter (Figure S2B). By EPR, the $m_s = -{}^3/_2$ hyperfine lines of both T1 Cu sites are present in approximately equal amounts (Figure 5B). The RFQ EPR data were also essentially the same as in the absence of Cl^- (Figure S3). Thus, Cl^- does not significantly alter the behavior upon reoxidation.

The rapid ET between the two T1 Cu sites provides convincing evidence that the $T1_{Remote}$ Cu site is able to participate in the ferroxidase mechanism. However, this reoxidation behavior is puzzling in one crucial regard: although the equilibration between the two T1 Cu sites is in agreement with the relative redox potentials of the Cu sites obtained from reductive titrations, the *lack* of ET to the trinuclear cluster after decay of the native intermediate state is not. One would expect the enzyme to equilibrate to the same electron distribution as seen upon addition of 1 equiv of Fe(II) to the oxidized enzyme (see Figure 2). This electron distribution is 1.6 oxidized T1 Cu, 0.4 oxidized T2 Cu, and 2.0 oxidized T3 Cu in the absence of Cl^- and 1.9 oxidized T1 Cu, 0.35 oxidized T2 Cu, and 1.75 oxidized T3 Cu in the presence of Cl^-. Since this is clearly not the case (the discrepancy is most apparent in the presence of Cl^-), it appears that, upon reduction and reoxidation with O_2, a "trapped" or nonequilibrium state of the enzyme is generated. Since there are no changes to the spectral features of the Cu sites in this nonequilibrium state, it appears to arise as a result of poising all of the enzyme molecules in a state in which the trinuclear Cu cluster is fully oxidized and only one T1 Cu is reduced.

2. The "Trapped" State. When Cp in phosphate buffer plus Cl^- is reduced with excess (6−8 equiv) Fe(II) and then reoxidized with O_2, a significantly greater fraction (~85%) of the blue band reappears within a few minutes (data not shown) than in the case of stoichiometric Fe(II) reduction. This implies that when >1 electron is available, ET to the trinuclear cluster now becomes possible, and the electron distribution among the

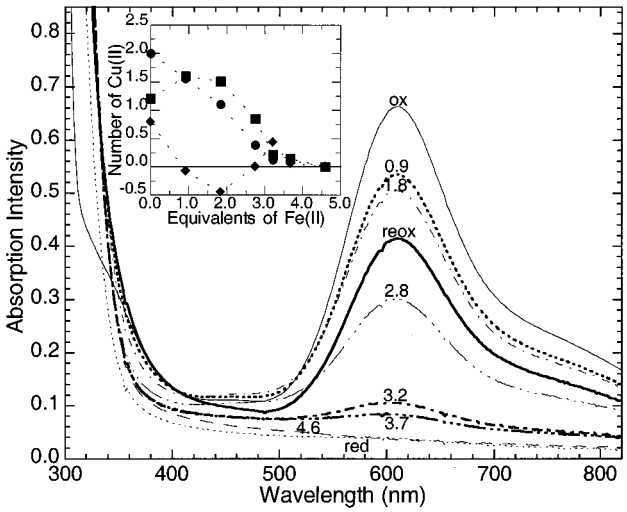

Figure 7. Absorption spectra of Cp in pH 7.0 phosphate buffer plus 0.15 M NaCl in the (—) resting oxidized, (- - -) reduced, (—) reoxidized with O_2, and then rereduced with the following: (- - -) 0.9, (—·—), 1.8, (—···) 2.8, (—•—) 3.2, (—•••) 3.7, and (— —) 4.6 equiv of Fe(II). Inset: Plot of the number of oxidized T1 (■), T2 (◆), and T3 (●) Cu sites upon reduction of the reduced-reoxidized "trapped" state with 0−4.6 equiv of Fe(II), as determined by the absorption data.

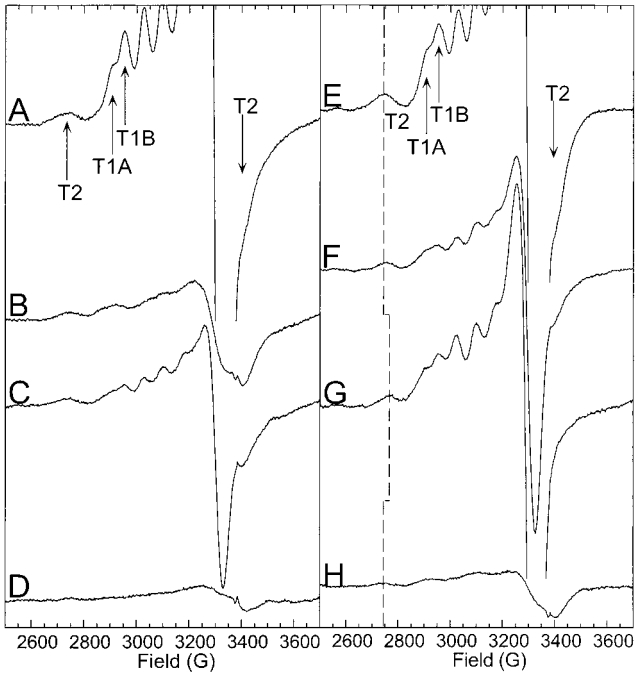

Figure 8. EPR spectra of human Cp in pH 7.0 phosphate buffer: (A) oxidized, (B) upon addition of 3.0 equiv of Fe(II) frozen after ∼45 s, (C) upon addition of 3.0 equiv of Fe(II) frozen after ∼30 min, and (D) upon addition of 6.0 equiv of Fe(II) frozen after ∼45 s. EPR spectra of human Cp in pH 7.0 phosphate buffer plus 0.15 M NaCl: (E) oxidized, (F) upon addition of 3.0 equiv of Fe(II) frozen after ∼45 s, (G) upon addition of 3.0 equiv of Fe(II) frozen after ∼30 min, and (H) upon addition of 6.0 equiv of Fe(II) frozen after ∼45 s. EPR conditions: microwave frequency, 9.482 GHz; temperature, 77 K; microwave power, 20 mW; modulation amplitude, 16 G; modulation frequency, 100 kHz; time constant, 0.5 s.

Cu sites approaches the equilibrium distribution observed in the reductive titrations. To further explore this, Cp in the trapped state in phosphate buffer plus Cl^- was generated, made anaerobic, and titrated with Fe(II). Absorption spectra of the oxidized, the reduced, the reduced−reoxidized trapped state, and the trapped state plus 0.9−4.6 equiv of Fe(II) are shown in Figure 7. These data demonstrate that, in the trapped state, the trinuclear cluster is fully capable of rereduction. Upon addition of ≥1.8 equiv of Fe(II) to the trapped state, the electron distribution among the Cu sites closely mirrors the results obtained previously in the reductive titration of the resting oxidized form (Figure 7, inset). Most importantly, upon addition of 0.9 and 1.8 equiv of Fe(II), the intensity of the blue band greatly *increases* (to 80 and 75%, respectively) above that of the nonequilibrium state (60%) (Figure 7, spectra labeled 0.9 and 1.8). *Thus, addition of a reductant induces oxidation of the T1 Cu.* This demonstrates that when ≥2 reducing equivalents are available in the system (one in the reduced-O_2−reoxidized trapped state distributed between the two T1 Cu sites and one or more equivalents of added reductant), ET from the T1 Cu to the trinuclear cluster can now occur, thus allowing reequilibration among the Cu sites. When the enzyme is poised with only one reducing equivalent on the T1 Cu, ET to the trinuclear cluster does not occur. This then explains the unusual behavior observed by de Ley and Osaki.[41]

3. Kinetics of ET upon Reduction with Fe(II). To understand the possible mechanistic origin of this kinetic trapping behavior, we examined the reduction kinetics of oxidized Cp by Fe(II) under two sets of conditions: substoichiometric Fe(II) (∼3 equiv) and excess Fe(II) (∼6 equiv). The latter probes whether slow steps exist in the reduction of the Cu sites. The former condition probes whether a slow reequilibration occurs among the Cu sites after the initial reduction event.

Reduction of Cp in phosphate buffer with ∼6 equiv of Fe(II) was examined by stopped-flow absorption. The 610-nm band bleached in <2 ms and the 360-nm band bleached in <100 ms (data not shown). Thus, upon addition of a slight excess of Fe(II), both the T1 Cu sites and the T3 Cu pair are reduced in an extremely rapid initial phase (k_{obs} > 1600 s^{-1} for the T1, k_{obs} > 23 s^{-1} for the T3). Next, the reduction of the T2 Cu upon addition of 6 equiv of Fe(II) was monitored by EPR. The EPR spectrum of a sample frozen at ∼45 s is shown in Figure 8D. It shows that, at 45 s, there is no oxidized T1 Cu but that there is still ∼0.16 oxidized T2 Cu (compare with the EPR spectrum of the resting oxidized state, in Figure 8A). At 30 min, the EPR spectrum showed no Cu signals.[61] This shows that, despite the very rapid reduction of T1 and T3 Cu by excess Fe(II), there is still a slow phase in the reduction of the T2 Cu site. Very similar results are obtained for Cp plus Cl^- reduced with 6 equiv of Fe(II) and frozen at ∼45 s (Figure 8H). This EPR spectrum shows that, at 45 s, all of the T1 Cu has reduced but that ∼0.31 T2 Cu remains oxidized. Again, the sample frozen at ∼30 min showed no Cu signals. This demonstrates that a slow phase exists in the reduction of the T2 Cu even upon addition of excess Fe(II).

The kinetic behavior of Cp in phosphate buffer upon addition of 3 equiv of Fe(II) was then examined by stopped-flow absorption to probe the subsequent reequilibration of electrons among the Cu sites. The absorption intensity at 610 and 360 nm was used to quantitate the amount of oxidized T1 and T3 Cu versus time, respectively, and the amount of oxidized T2 was estimated based upon mass balance (Figure 9A). These results show that all of the T1 Cu is reduced quickly (<0.1 s) and that there is a subsequent a slow phase ($t_{1/2}$ ∼10 min) in which a fraction of the T1 Cu is reoxidized. About 0.80 T3 copper is reduced quickly (<0.1 s), followed by a very slight

(61) As in the reductive titrations, an Fe(III) signal was present that was used to subtract out the Fe(III) signal of the other spectra.

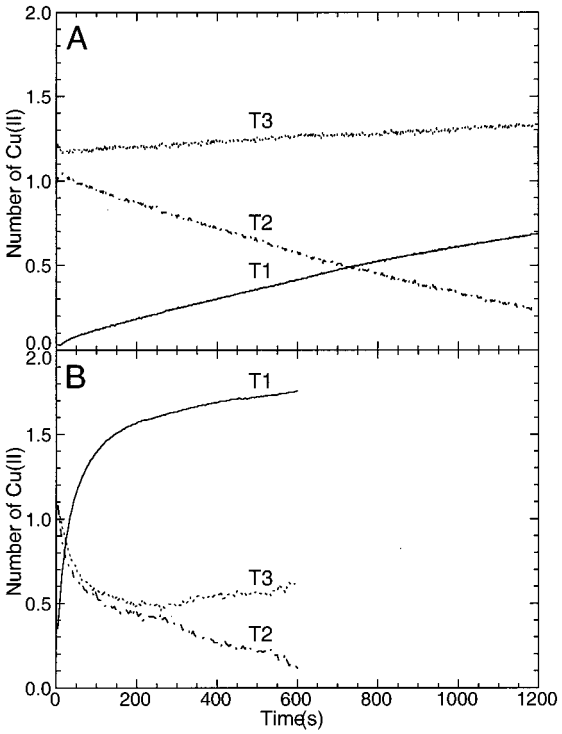

Figure 9. Stopped-flow absorption data of oxidized human Cp upon addition of ~3 equiv of Fe(II). The plots show the number of oxidized T1 (—), T2 (- - -), and T3 (—•—) Cu versus time. Amounts of T1, T2, and T3 Cu before addition of reductant are 2.0, 1.0, 2.0, respectively (i.e., initial reduction phase is too fast to see on this time scale). Conditions: (A) in pH 7.0 phosphate buffer; (B) in pH 7.0 phosphate buffer plus 0.15 M NaCl.

Table 2. Number of Oxidized T1 and T2 Cu Sites in Human Cp in Phosphate Buffer upon Addition of Fe(II)

conditions	oxidized T1 Cu	oxidized T2 Cu
no Cl^-		
3 equiv of Fe(II), ~45 s	<0.25	0.59
3 equiv of Fe(II), 30 min	0.37	0.57
6 equiv of Fe(II), ~45 s	0.0	0.16
with Cl^-		
3 equiv of Fe(II), ~45 s	0.57	0.51
3 equiv of Fe(II), 30 min	1.25	0.75
6 equiv of Fe(II), ~45 s	0.0	0.31

increase in the amount of oxidized T3 Cu. By mass balance, essentially all of the T2 Cu is reduced very slowly, with the same $t_{1/2}$ as the slow reoxidation phase observed for the T1 Cu. EPR was used to monitor the T1 and T2 Cu signals as a function of time. Traces B and C of Figure 8 show the EPR spectra of Cp upon addition of 3 equiv of Fe(II) frozen after ~45 s and frozen after 30 min. The EPR spectrum of the 45-s sample (Figure 8B) shows very little oxidized T1 Cu (<0.25) and ~0.59 oxidized T2 Cu. The EPR spectrum of the 30-min sample (Figure 8C) shows that the amount of oxidized T1 Cu has increased to 0.37 Cu. This is in agreement with the absorption data, indicating a fast reduction of the T1 Cu sites, followed a slow reoxidation phase. Also, the spectrum in Figure 8C shows that, at 30 min, the amount of oxidized T2 Cu is essentially unchanged (0.57 Cu). These data are summarized in Table 2.

Since Cl^- affects the redox potentials of the Cu sites, the effect of 0.15 M NaCl on the kinetic behavior of reduction of anaerobic oxidized Cp by Fe(II) was examined. The amount of oxidized T1 Cu versus time upon addition of ~3 equiv of Fe(II) determined by stopped-flow absorption is shown in Figure 9B. Essentially all of the T1 Cu is reduced quickly (<0.1 s), followed by a slow phase in which most of the T1 Cu is reoxidized. This slow phase is much faster ($t_{1/2}$ ~30 s) than in the absence of Cl^-. Also, these data show that 1.0 T3 copper reduces quickly (<0.1 s), and an additional 0.5 T3 Cu reduces in a slower phase. Essentially all of the T2 Cu reduces slowly. Traces F and G of Figure 8 show the EPR spectra of Cp plus Cl^- reduced with 3 equiv of Fe(II) frozen after ~45 s and 30 min. The EPR spectrum of the 45-s sample exhibits ~ 0.57 oxidized T1 Cu (Figure 8F). Since the T2 Cu EPR spectrum changes upon reduction of the T3 Cu in the presence of Cl^- (vide supra), the amount of oxidized T2 Cu was determined by double integration followed by subtraction of the fraction of oxidized T1, as was done for the reductive titrations. From this, 0.51 oxidized T2 Cu remains at ~45 s. At 30 min, the amount of oxidized T1 Cu has increased to 1.25 Cu, in agreement with the absorption results in Figure 9B. The T2 Cu signal in sample frozen at 30 min (Figure 8G) shows several changes relative to that of the 45-s sample: the amount of T2 Cu has increased to 0.75 Cu, the $m_s = -3/2$ hyperfine peak has shifted to higher field by ~20 G, and the prominent off-axis turning point seen at ~3405 G has disappeared. These changes are the same as observed in the reductive titration data between the 0-equiv and the 2.0-equiv Fe(II) samples. Since by mass balance the reoxidation of the T1 and T2 Cu sites must be concomitant with reduction of the T3 Cu pair, this demonstrates that the shift in the T2 Cu EPR signal occurs upon reduction of the T3 Cu. Thus, the kinetics of reduction of Cp with Cl^- has several features in common with that of Cp without Cl^-: a fast initial phase of reduction of the T1 and T3 Cu sites followed by a slow phase of ET from the T1 Cu to the trinuclear cluster.

To summarize, the kinetics of reduction of Cp with substoichiometric Fe(II) in phosphate buffer both with and without Cl^- exhibits a fast reduction of both the T1 Cu and a fraction of the T3 Cu. Subsequently, there is a slow phase consisting of ET from the T1 Cu to the trinuclear cluster (the T2 and/or T3 Cu sites, depending upon the conditions).

Discussion

The Mechanism of Intramolecular ET. This study provides the first comprehensive picture of the thermodynamics and kinetics of intramolecular ET in Cp. We have shown that, under physiologically relevant conditions, the redox potentials of the two T1 Cu sites are the same and that Cl^- is an important effector of the electron distribution between the T1 Cu sites and the trinuclear cluster under equilibrium conditions. Upon reoxidation of fully reduced Cp with O_2, RFQ EPR data show that ET from the $T1_{Remote}$ Cu site to the $T1_{CysHis}$ Cu site occurs at >150 s^{-1}. Reduction of the T1 Cu sites by Fe(II) is extremely rapid (k_{obs} > 1600 s^{-1}), as is reduction of the T3 Cu pair, as shown by stopped-flow absorption. With excess Fe(II), reduction of the T2 Cu is the slowest step, as shown by EPR. With substoichiometric Fe(II), the slow phase of reduction of the T2 Cu correlates with the slow reoxidation phase of the T1 Cu. Addition of Cl^- increases the rate of this slow phase. When the enzyme is poised with only one reducing equivalent on the T1 Cu, ET to the trinuclear Cu cluster does not occur, despite the favorable driving force for this in the presence of Cl^-. Addition of 1−2 equiv of Fe(II) to this trapped state *induces ET from the T1 Cu to the trinuclear cluster, leading to a net oxidation of T1 Cu*. Thus >1 electron is required in order to reduce the trinuclear cluster.

The above large body of thermodynamic and kinetic data can be used to evaluate possible models for the mechanism of intramolecular ET in Cp, yielding important insights that are

broadly applicable to the class of multicopper oxidases as a whole. The simplest possible mechanism for intramolecular ET in Cp that includes all feasible steps is shown in Scheme 2.

Scheme 2

step 1: $Fe_R + T1Rm_O \overset{K_1}{\rightleftharpoons} Fe_O + T1Rm_R$

step 2: $Fe_R + T1CH_O \overset{K_2}{\rightleftharpoons} Fe_O + T1CH_R$

step 3: $T1Rm_R + T1CH_O \overset{K_3}{\rightleftharpoons} T1Rm_O + T1CH_R$

step 4: $Fe_R + T1CH_R + T3_O \overset{K_4}{\rightleftharpoons} Fe_O + T1CH_O + T3_R$

step 5: $T1Rm_R + T1CH_R + T3_O \overset{K_5}{\rightleftharpoons} T1Rm_O + T1CH_O + T3_R$

step 6: $T1CH_R + T2_O \overset{K_6}{\rightleftharpoons} T1CH_O + T2_R$

step 7: $T3_R + T2_O + T1CH_O \overset{K_7}{\rightleftharpoons} T3_O + T2_R + T1CH_R$

In this scheme, the $T1_{Remote}$ and $T1_{CysHis}$ Cu sites are abbreviated as T1Rm and T1CH, respectively, and the subscripts R and O designate reduced and oxidized, respectively.

Steps 1 and 2 are the reduction of the T1 Cu sites by Fe(II). All available evidence indicates that the T1 Cu site in multicopper oxidases is the site of substrate oxidation,[1] and in Cp, the proximity of the divalent metal ion binding (M^{2+}) sites to the T1 Cu sites further supports this idea.[10,11] The kinetic data show that this site is very rapidly reduced upon addition of Fe(II). Thus, these steps are clearly justified in the mechanism, and the rates $k_{1\rightarrow}$ (forward rate constant for step 1) and $k_{2\rightarrow}$ should be very large. Step 3 is the intramolecular ET between the two T1 Cu sites. From RFQ EPR, we have shown that this rate is relatively fast, with a lower limit of 150 s^{-1}.

Andréasson and Reinhammar proposed that, in plant Lc, after the T1 Cu site is reduced, another substrate molecule reduces the T2 Cu site, and together, these reduce the T3 Cu pair by two electrons (reverse of step 7 above).[23] The crystal structures of the multicopper oxidases show that the T2 Cu site is quite buried, and indeed, we find no evidence for a viable ET pathway from the M^{2+} site to the T2 Cu in Cp. Furthermore, in Cp upon addition of excess Fe(II), the T3 Cu reduces in <100 ms, while a significant fraction of T2 Cu is still evident by EPR after 45 s. We propose an alternative mechanism consistent with the data: a reduced T1 Cu and another Fe(II) together reduce the T3 Cu pair (step 4). Such a mechanism could occur in two steps: an equilibrium could exist between a reduced T1 Cu and a half-met T3 with the reduced T1 Cu heavily favored (since no half-met T3 Cu is observed by EPR); addition of another electron from Fe(II) drives the half-met T3 to complete reduction. The presence of the M^{2+} site adjacent to the T1 Cu site in Cp makes step 4 particularly appealing. Another possible mechanistic step for reduction of the T3 Cu pair would be that both T1 Cu sites transfer electrons to the T3 Cu pair (step 5), again possibly in a two-step process. Given that the initial reduction of the T3 Cu is quite fast, step 5 is not likely to be the initial reduction step, but could be responsible for subsequent slower ET steps.

The existence of the trapped state and the requirement of an additional equivalent of reductant to allow ET to the trinuclear cluster demonstrates that reduction of the trinuclear cluster requires two electrons. Given that the T3 Cu acts as a two-electron acceptor, and that kinetically reduction of the T2 Cu always occurs after reduction of at least a fraction of the T3 Cu, it is logical that the T3 Cu pair plays a defining role in the mechanism of reduction of the trinuclear cluster. Thus, the redox behavior of the trinuclear cluster is coupled, and the T3 Cu pair functions in gating ET to the tricopper cluster. Some evidence for such communication between the T2 and T3 Cu sites already exists from the change in the EPR parameters of the T2 Cu site in the presence of Cl^- upon reduction of the T3 Cu pair. Such a coupling could be either geometric or electronic in nature. Among the possibilities are a subtle direct geometric perturbation to the T2 Cu upon redox of the T3 Cu or a change in the electrostatic environment due to charge differences. Several mechanistic steps for reduction of the T2 Cu may be involved. Step 7, in which a reduced T3 Cu pair reduces the T2 Cu and the $T1_{CysHis}$ Cu, is a particularly attractive possibility and provides a direct means whereby the redox behavior of the trinuclear cluster is coupled. In this mechanistic step, the reduction of the T2 Cu also requires an oxidized T1 Cu. Upon addition of excess Fe(II), at least a fraction of the T2 Cu reduces slowly, even though the T1 Cu was rapidly reduced. Therefore, in this case, an additional factor generating this slow step must be present. An alternative mechanistic step for reduction of the T2 Cu site is a slow direct ET from the $T1_{CysHis}$ Cu (step 6). This would account for the slow reduction of the T2 Cu and the slow reoxidation phase of the T1 Cu. Modulation of the T2 Cu site by the redox state of the T3 Cu would then explain the requirement of two electrons for reduction of the trinuclear cluster even with such a step operative.

Intramolecular Electron-Transfer Pathways. Further insight into the nature of intramolecular ET in Cp can be obtained from analysis of possible ET pathways. We have used the isotropic model (see Experimental Section) to obtain approximate theoretical estimates of various ET factors for the different mechanistic steps and the Pathways program[48−56] to compare relative efficiencies of ET rates among different pathways for each step.

1. The M^{2+} to the T1 Pathway. In both domains 4 and 6, the M^{2+} site is quite close to the T1 site: 8.9 Å. In domain 6, the ligands for the M^{2+} site are His940, Glu272, Asp1025, and Glu935. The same binding motif is also found in domain 4. The first three ligands are in close proximity to the ligands of the $T1_{CysHis}$ site. Thus, it is not surprising that this ET step is fast: in the reduction of the enzyme, the apparent first-order rate constant is >1600 s^{-1}. The best ET pathway identified by the Pathways program travels from Glu272 Oϵ2 to the other O of the carboxylate, then across an H-bond to His1026 Hϵ2, and then along the imidazole ring to the $T1_{CysHis}$ Cu. This gives a total decay coupling of 2.8×10^{-2}. Two alternative pathways also give favorable decay couplings: either from Asp1026 or His940 across a space jump to His1026 Hδ2. These pathways are illustrated in Figure 10A. Analogous M^{2+} to T1 pathways also exist in domain 4. Pathways from the M^{2+} site to the trinuclear cluster were also examined. All reasonable possibilities included the $T1_{CysHis}$ site or ligands thereof and so this ET step was not further considered. Relative pathway efficiencies can be compared by converting the total decay coupling into a nonintegral number of covalent bonds, n, which in turn can be converted into an effective total covalent bond distance, σ_l, by multiplying by 1.4 Å. This can be compared to the actual distance and from there a β-value can be derived.[46,53] In this way, the decay coupling of the above pathway converts to a β

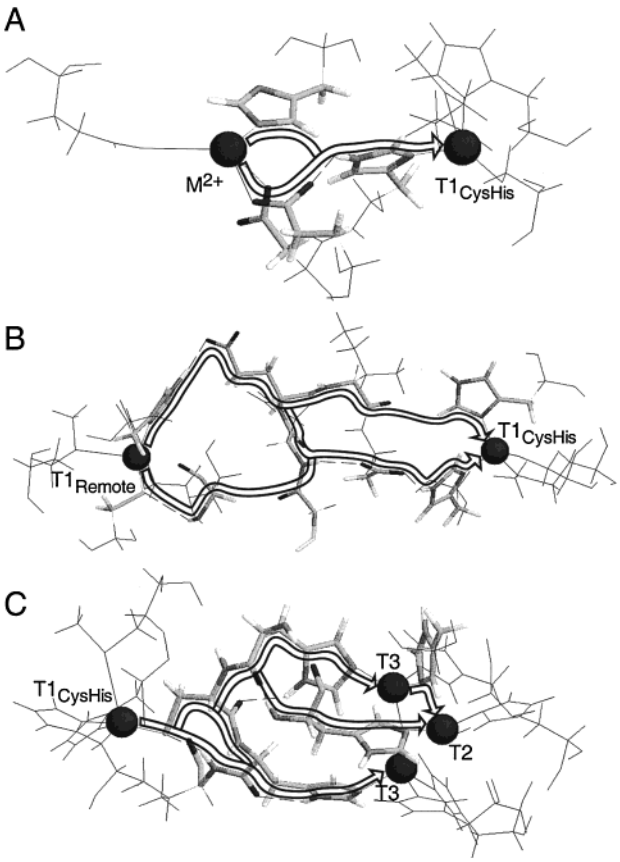

Figure 10. Illustration of the various ET pathways in Cp, taken from the X-ray crystal structure (ref 10, accession number 1KCW) and calculated with the Pathways program. (A) The M^{2+} site to $T1_{CysHis}$ Cu site ET pathways. (B) The $T1_{CysHis}$ Cu site to $T1_{Remote}$ Cu site ET pathways. (C) The $T1_{CysHis}$ Cu site to trinuclear Cu cluster ET pathways.

of 1.18 $Å^{-1}$. Although the driving force for this reaction is not known, the fact that reduction of Cp with Fe(II) is stoichiometric indicates that the redox potential of bound Fe(II) must be quite low, at least 200 mV lower than the Cu redox potentials. Given the favorable coupling and appreciable driving force, it is clear that this ET step will be rapid even if the reorganization energy of the bound Fe is large.

2. The $T1_{Remote}$ to $T1_{CysHis}$ Pathway. Two possibilities exist for the fairly rapid reoxidation of the $T1_{Remote}$ Cu site: direct $T1_{Remote}$ to trinuclear cluster ET or $T1_{Remote}$ to $T1_{CysHis}$ ET. We examined the former possibility using Pathways. The best pathways included the $T1_{CysHis}$ Cu site or ligands thereof. By deliberately excluding such possibilities, several other possible pathways were obtained, but all were far worse than the $T1_{Remote}$ to $T1_{CysHis}$ pathways and were not further considered. Given the Cu−Cu distance of 17.9 Å, assuming a β of 1.0 $Å^{-1}$ (vide infra) and a λ equal to that of the blue Cu site of Az, 0.8 eV, the predicted ET rate is 1500 s^{-1}, consistent with the experimental lower limit of 150 s^{-1}. The Pathways program yielded several viable $T1_{Remote}$ to $T1_{CysHis}$ ET pathways. The best pathway travels from His685 to Glu971 Oϵ2 via an H-bond, then an all-covalent path to the Ile972 O, and then to His1026 Hϵ1 via a 2.58-Å space jump. The overall decay coupling is 2.5×10^{-5}. This pathway is essentially the same as the T1 to T1 ET pathway identified by Farver, Pecht, and co-workers,[42] except the latter included a very long 3.37-Å Ile972 O to His1026 Hϵ2 H-bond. Another reasonable option travels from His685 to Glu971 Oϵ2, then along an all-covalent pathway to Asn970 NH, then to Asp973 Oδ2 via an H-bond, then to Asp973 Oδ1, and then an across an H-bond to His 975. This pathway is longer but still has a decay coupling of 1.7×10^{-5}. The third good option travels from Cys680 Sγ across an H-bond to Thr682 NH, then to Thr682 Cα, then across a 2.35-Å space jump to Gly969 O, and then to Asn970 NH. From there, the rest of the pathway is the same as the one above. This pathway yields a decay coupling of 1.2×10^{-5}. These pathways are illustrated in Figure 10B, and the relevant information is summarized in Table 3. Taking the best of the above pathway gives a calculated β of 1.40 $Å^{-1}$. Using this value of β in the isotropic model yields a predicted ET rate of 4 s^{-1}, which is less than the experimental lower limit but reasonable given the level of theory and the many assumptions made. In particular, one would predict that the reorganization energy of the T1 Cu sites in Cp would be lower than in Az. The reorganization energy comprises two terms, an inner-sphere term, dictated by the ligands, and an outer-sphere term. A major contribution to the latter is solvent reorganization. Since in contrast to Az, the T1 Cu sites of Cp are not solvent-exposed, the outer-sphere term is predicted to be lower. This would offset the less than optimal electronic coupling between the T1 Cu sites.

Table 3. Comparison of Cu−Cu Distances from Crystallography and Relative Decay Couplings from Pathways[53−61] Analysis for Various Intramolecular ET Pathways in Cp

pathway	distance (Å)	exptl rate (s^{-1})	best rel bridge decay coupling	calcd β ($Å^{-1}$)
M^{2+} to T1	8.9	>1600[a]	2.8×10^{-2}	1.18
$T1_{Remote}$ to $T1_{CysHis}$	17.9	>150		
His685 to His1026			2.5×10^{-5}	1.40
His685 to His975			1.7×10^{-5}	
Cys680 to His975			1.2×10^{-5}	
$T1_{CysHis}$ to T3	12.5	>23[a]		
down Cys1021 side chain			6.0×10^{-3}	1.04
H-bond to Cys1021 Sγ			6.3×10^{-3}	
T3 to T2	4.2	na[b]	1.1×10^{-1}	na
$T1_{CysHis}$ to T2	14.4	0.023[c]	1.3×10^{-3}	1.14

[a] Apparent first-order rate constant at a protein concentration of 10 μM. [b] na, not available. [c] Approximated based upon the slow phase of reoxidation of the T1 Cu from stopped-flow absorption in the presence of Cl^- and from the EPR data, assuming a purely first-order $T1_{CysHis}$ to T2 Cu ET;.

3. The $T1_{CysHis}$ to T3 Pathway. The stopped-flow absorption data on the kinetics of reduction upon addition of excess Fe(II) showed that the T3 Cu reduced in 100 ms. As discussed previously, the most logical mechanistic step to account for this fast rate involves a reduced T1 Cu and a bound Fe(II) together reducing the T3 by two electrons either in a concerted or a two-step process. Note that, in plant Lc, the T1 to T3 ET rate upon formation of the native intermediate has been estimated at >1000 s^{-1} based upon comparison of the rates of formation of the peroxide-level and the native intermediates. The Pathways program yielded several good $T1_{CysHis}$ to T3 ET pathways. The best pathway travels from Cys1021 Sγ to Val1023 NH via a 2.64-Å H-bond, followed by an all-covalent pathway to His1022, a ligand of the T3 Cu (Figure 10C). This gives a total decay coupling of 6.3×10^{-3}. Alternatively, a slight modification of this pathway yields the same decay coupling: instead of traveling from Val1023 NH along the backbone to the side chain of His1022, an H-bond skips from His1022 O to the Hδ1 atom on the imidazole ring. Another good pathway travels from Cys1021 Sγ, down the side chain of Cys1021 to the backbone and then down the side chain of His1022. This all-covalent pathway yields a coupling of 6.0×10^{-3}. The analogous pathway down the side chain of His1020 to the other T3 Cu ion has the same coupling. These pathways are illustrated in

Figure 10C. These latter two pathways were previously identified in Cp by Farver et al.,[42] and the analogous pathways were identified in AO several years ago.[62,63] The first pathway, which in Cp includes a Val1023 NH to Cys1021 Sγ H-bond, has not been previously identified in the multicopper oxidases. In the crystal structures of both AO and fungal Lc, the analogous pathway indeed exists; therefore, we conclude that this is a viable T1 to T3 ET pathway in these systems as well. The decay coupling of this pathway in Cp (6.3×10^{-3}) converts to a β of 1.04 Å^{-1}. This indicates that even if the reorganization energy of the T3 Cu site is high, which is implied from the crystal structure data,[7,8] this will still be a very fast pathway.

4. Pathways to the T2. Two types of ET paths to the T2 Cu site must be considered: pathways from the T3 Cu pair and direct $T1_{CysHis}$ to T2 pathways. The best T3 to T2 pathway travels from one of the T3 coppers along its ligand His980 to the Hδ2 atom on the imidazole ring and then across a 1.6-Å space jump directly to the T2 Cu (Figure 10C). This yields a very strong decay coupling of 0.11 (Table 3). The best pathway from the other T3 Cu to the T2 Cu was along the hydroxide bridge to the first T3 Cu and then into the same pathway. Even assuming large values for the reorganization energies of the T2 and T3 Cu sites, this would still be a highly efficient ET pathway.

A good $T1_{CysHis}$ to T2 pathway also exists: from Cys1021 Sγ along the Cys side chain to the Cys1021 N, then to the His1020 O, then across an H-bond to His978 NH, and from there to the T2 Cu (Figure 10C). This yields a decay coupling of 1.3×10^{-3} (Table 3), which in turn converts to a β of 1.14 Å^{-1}. This indicates that the inability of T1 Cu to transfer electrons to the T2 Cu in the trapped state cannot be explained by the lack of a direct ET pathway, which in turn, further shows that reduction of the T2 Cu site must be directly coupled to reduction of the T3 Cu pair.

5. The Effect of Metal−Ligand Bonding on ET Pathways. In the ET pathways of Cp, three types of pathways involving the T1 Cu were found: through the $Cu-N_{His}$ bond, through the $Cu-S_{Cys}$ bond then down the Cys side chain, and through the $Cu-S_{Cys}$ bond and then across an H-bond to an amide N. The anisotropy of the T1 Cu metal−ligand bonding necessitates an examination of the effect of these differences on the ET rate. In the McConnell superexchange mechanism, the effect of coupling in to and out of the bridge on H_{AB} is incorporated into the prefactor, $(H_{12})(H_{m+1,m+2})/\Delta E_{12}$. In comparing mechanisms of coupling into a given bridge in which the zeroth-order final state and the coupling of the bridge to the final state are kept the same, the term to consider is $H_{12}/\Delta E_{12}$, where H_{12} is the metal−ligand resonance integral and ΔE_{12} is the ligand to metal charge-transfer energy. $H_{12}/\Delta E_{12}$ is equal to the semioccupied molecular orbital (SOMO) wave function coefficient, which, in turn, is equal to the square root of the covalency. Thus, for a given bridge and final state, k_{ET} is proportional to the metal−ligand covalency. From density function theory (DFT) calculations on the blue Cu site of plastocyanin (Pc),[2,3,64,65] which is structurally and spectroscopically very similar to the T1 Cu site in the multicopper oxidases, the redox-active $d_{x^2-y^2}$ orbital has 38% S_{Cys} and 2−5% N_{His} character. This has also been directly quantitated by S K-edge X-ray absorption spectroscopy (XAS) and found to be in agreement with the DFT results.[66] Therefore, in comparing ET pathways involving the T1 Cu site, pathways through the $Cu-S_{Cys}$ bond will be at least a factor of ~10 faster.

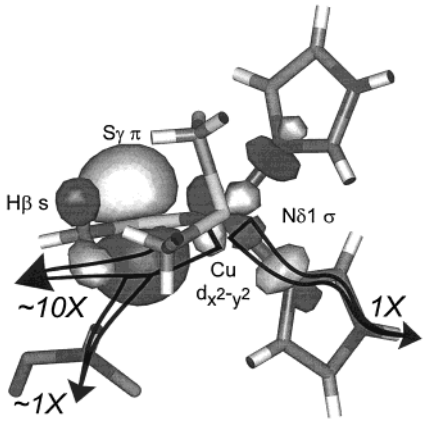

Figure 11. Illustration of the three mechanisms of coupling from the Cu $d_{x^2-y^2}$ orbital into the bridge: through the histidine Nδ1, hyperconjugation through the Cys Sγ to the Cys Hβs, or though the Cys Sγ across an H-bond to the backbone amide N. The Cu site structure shown is Pc, and the wave function plot is that of Pc calculated with ADF. The backbone amide is positioned to be aligned with the $Cu-S_{Cys}$ moiety as the Val1026 backbone amide is in the $T1_{CysHis}$ site of Cp.

Additional insight can be gained from examining the delocalization of the SOMO wave function further out onto the ligands from both DFT calculations and experimental data on blue Cu sites. In particular, the coupling of the Cys Sγ orbitals with the next step in the pathway, either the Cys β-methylene or the H-bonded amide NH, is of interest. Since the Cys Sγ orbital in the SOMO is a π orbital and ET in proteins is assumed to be via σ-type pathways, one possibility is coupling between the Sγ π and σ orbitals, where the σ orbital is the S−C bonding level. Since these are orthogonal, this would have to be through spin−orbit coupling:

$$\propto \left(\lambda \frac{\langle p_\pi | LS | p_\sigma \rangle}{\Delta E}\right)^2 \qquad (6)$$

From DFT calculations, ΔE is 5.3 eV, so this term is very small and thus direct S π to σ coupling is not a viable means of further coupling along the Cys pathway. However, very large positive hyperfine couplings (16−28 MHz) have been experimentally observed for the Cys Hβs in Pc and Az from continuous-wave Q-band electron nuclear double-resonance spectroscopy (ENDOR)[67] and paramagnetic proton nuclear magnetic resonance spectroscopy (^{1}H NMR).[68,69] By comparison with the Cu−S−C−Hβ dihedral angles from X-ray crystallography, the dominant mechanism of spin delocalization is direct π delocalization from the Cys Sγ, i.e., hyperconjugation, rather than spin polarization. The magnitude of the hyperfine coupling yields spin densities of 1.6 and 1.2% for each of the Cys Hβs. This compares very favorably with the total spin density of 2.7% for the Cys Hβs calculated from DFT, pictured in Figure 11. Therefore, hyper-

(62) Meyer, T. E.; Marchesini, A.; Cusanovich, M. S.; Tollin, G. *Biochemistry* **1991**, *30*, 4619−4623.
(63) Farver, O.; Pecht, I. *Proc. Natl. Acad. Sci. U.S.A.* **1992**, *89*, 8283−8287.
(64) Guckert, J. A.; Lowery, M. D.; Solomon, E. I. *J. Am. Chem. Soc.* **1995**, *117*, 2817−2844.
(65) LaCroix, L. B.; Shadle, S. E.; Wang, Y.; Averill, B. A.; Hedman, B.; Hodgson, K. O.; Solomon, E. I. *J. Am. Chem. Soc.* **1996**, *118*, 7775−7768.
(66) Shadle, S. E.; Penner-Hahn, J. E.; Schugar, H. J.; Hedman, B.; Hodgson, K. O.; Solomon, E. I. *J. Am. Chem. Soc.* **1993**, *115*, 767−776.
(67) Werst, M. M.; Davoust, C. E.; Hoffman, B. M. *J. Am. Chem. Soc.* **1991**, *113*, 1533−1538.
(68) Bertini, I.; Ciurli, S.; Dikiy, A.; Gasanov, R.; Luchinat, C.; Martini, G.; Safarov, N. *J. Am. Chem. Soc.* **1999**, *121*, 2037−2046.
(69) Bertini, I.; Fernandez, C. O.; Karlsson, B. G.; Leckner, J.; Luchinat, C.; Malmström, B. G.; Nersissian, A. M.; Pierattelli, R.; Shipp, E.; Valentine, J. S.; Vila, A. J. *J. Am. Chem. Soc.* **2000**, *122*, 3701−3707.

conjugation to the Cys Hβs provides a highly efficient mechanism for coupling along the Cys side chain.

The final possibility to consider is coupling through the H-bond to the backbone amide. Comparison of the structures and amino acid sequences of blue Cu proteins and multicopper oxidases yields a notable pattern in backbone amides H-bonded to the Cys Sγ. Az has two H-bonded backbone amides: one residue downstream of the His ligand (Asn47) and two residues downstream of the Cys ligand (Phe114). Pc, pseudoazurin, and amicyanin have only one H-bonded amide, one residue downstream of the His ligand (Asn38 in Pc), while two residues downstream of the Cys is a Pro. In Cp, all three T1 Cu sites have two H-bonded amides: one residue downstream of the His ligand (Thr976 in domain 6) and two residues downstream of the Cys ligand (Val1023 in domain 6). AO and fungal Lc, and by sequence comparisons all of the other multicopper oxidases, have only one H-bonded amide: one residue downstream of the His ligand is a Pro, while two residues downstream of the Cys is an H-bonded amide (Ile509 in AO). The latter amide appears as a possible ET pathway in all of the multicopper oxidases.

Pulsed W-band ENDOR on globally ^{15}N-labeled single-crystal Az has detected spin density on three backbone amides, as well as the remote (ϵ2) Ns of the His ligands.[70] The isotropic hyperfine shifts for the two His Nϵ2s were 1.30 and 0.87 MHz and for the three amide Ns were 0.95, 0.55, and 0.22 MHz. Those of the His Nδ1s in Pc and Az by Q-band ENDOR are 22 and 22 MHz and 27 and 17 MHz, respectively. From the hyperfine shifts assigned to His46 in Az, 17 MHz for Nδ1 and 0.87 MHz for Nϵ2, spin densities of 4.9 and 0.24% were calculated, respectively.[70] This compares favorably with spin densities from DFT calculations on the His Ns of Pc (4.5 and 0.2%). This shows that the His rings are far less efficient at spin delocalization than the Cys Hβs. Of the three backbone amides detected by pulsed W-band ENDOR, one was assumed to be the Cys amide N, and the other two were not assigned. We suggest that these two are the H-bonded amides, Phe114 and Asn47. By comparison of the isotropic hyperfines of the backbone amides with the His Nϵ2s, the spin densities on the amides are approximately $1-{}^1/_4$ that of the His Nϵ2s. This indicates that although the H-bond to the Cys Sγ provides a possible means of coupling into the ET pathway, it is not as favorable as coupling along the Cys side chain.

In summary, ET pathways through the Cys Sγ and down the side chain will be at least ~10-fold faster than pathways through the His Nδ1 due to the anisotropic covalency of the T1 Cu SOMO. Theory and experiment both support that the pathway down the Cys side chain travels via hyperconjugation to the Cys Hβs and not via spin−orbit mixing of the Cys π and σ orbitals and that the very large degree of spin delocalization to the Cys Hβs indicates that this path is probably significantly more than 10-fold more efficient than the His Nδ1 pathway. This shows why T1 to T3 ET along the CysHis linkage is fast and why this linkage is evolutionarily conserved among all the multicopper oxidases to provide efficient four-electron reduction of O_2 at the trinuclear cluster. Coupling through the Cys Sγ to amide H-bond is probably comparable to the pathways involving the His Nδ1. These pathways are illustrated in Figure 11. Although the H-bond is a viable pathway for T1 to T3 ET, it probably does not dominate. Also, this means that all three $T1_{Remote}$ to $T1_{CysHis}$ pathways in Figure 10B, two that travel through the His and one that travels through the Cys Sγ to amide, are probably comparable. Although the ET rate advantage of the anisotropic covalency of the T1 sites is not being optimally exploited in this case, this ET pathway need not be as efficient: it is not essential for either the oxidation of Fe(II) or for the reduction of O_2. It may, however, still serve a useful function in the overall ferroxidase activity of Cp.

Implications for the Ferroxidase Mechanism. The RFQ EPR data demonstrates that the $T1_{Remote}$ to $T1_{CysHis}$ ET rate is quite fast ($>150\ s^{-1}$) despite the long distance of 17.9 Å. The reductive titration data demonstrated that these Cu sites have the same potential. The k_{cat} for Fe(II) from steady-state kinetics has been reported to be 138 or 550 min^{-1}.[57,58] Therefore, the $T1_{Remote}$ Cu site fulfills both requirements for potential catalytic relevance. Yet, it is not needed for O_2 reduction. The proposed role of Cp in Fe metabolism puts unique constraints on its function as an enzyme. The concentration of free Fe(II) in plasma is generally considered to be vanishingly small. Thus, it has been assumed that Cp obtains Fe(II) from some as yet unidentified membrane-bound Fe(II) pump. The protein to which Cp delivers Fe(III) is transferrin (Tf), which is a soluble plasma protein. Unless the delivery of Fe involves a ternary complex, this means that the uptake and delivery of Fe by Cp are spatially separated. Thus, in vivo the overall rate-limiting step for Cp could be Fe delivery to Tf, in which case Cp could be acting as a short-range Fe(III) transporter. After Cp is fully reduced by Fe(II), it will presumably be rapidly reoxidized by O_2 and then deliver Fe(III) to Tf. The crystal structure of Cp shows that domains 6 and 4 each contain a T1 Cu site, a divalent metal ion binding site (M^{2+}) and a trivalent metal ion binding site (M^{3+}). If each domain is capable of tightly binding two Fe(III) ions, either by keeping one in the M^{2+} site or by having both Fe(III) ions bound at the M^{3+} site, as postulated by Lindley and co-workers,[11] a single molecule of Cp could sequester four Fe ions in a single interaction event with the membrane-bound Fe(II) pump. This would minimize the buildup of partially reduced Cp species. Thus, the $T1_{Remote}$ Cu site is not needed for oxidase activity, but may be important in increasing overall Fe metabolism efficiency.

Acknowledgment. We thank the following for their contributions to this work: the Stanford Blood Center for providing human plasma, Dr. Sang-Kyu Lee for helpful discussions on kinetics and help is setting up the RFQ apparatus, Liliana Quintanar and Amy Palmer for obtaining the stopped-flow absorption data with a 2-ms dead time, Dr. David Randall for helpful discussions on ET and in particular on the importance of the Cys Hβs, Pierre Kennepohl for helpful discussions on ET, Dr. Regan at Cal Tech for providing us with the Pathways program, and Joe Barco and Prof. Tom Wandless for use of Insight II. This research was supported by NIH Grant DK31450. T.E.M. was supported by an NSF predoctoral fellowship and a Stanford University Leiberman Fellowship.

Supporting Information Available: Figures of the reductive titrations of human Cp in MOPS buffer, the absorption spectra of Cp upon reoxidation with O_2, and the RFQ EPR spectra of O_2-reoxidized human Cp in phosphate buffer with Cl^- (PDF). This material is available free of charge via the Internet at http://pubs.acs.org.

JA002339R

(70) Coremans, J. W. A.; Poluektov, O. G.; Groenen, E. J. J.; Canters, G. W.; Nar, H.; Messerschmidt, A. *J. Am. Chem. Soc.* **1996**, *118*, 12141−12153.